International Journal of Nanomedicine

Dovepress
open access to scientific and medical research

Open Access Full Text Article

ORIGINAL RESEARCH

Inflammatory Genes Associated with Pristine Multi-Walled Carbon Nanotubes-Induced Toxicity in Ocular Cells

Xiaogang Luo[1], Dongli Xie[1], Jing Su[2], Jianchen Hu[1]

[1]College of Textile and Clothing Engineering, Soochow University, Suzhou, 215123, People's Republic of China; [2]Shanghai Institute of Spacecraft Equipment, Shanghai, 200240, People's Republic of China

Correspondence: Xiaogang Luo; Jianchen Hu, Tel +86-0512-67162531, Email xgluo@suda.edu.cn; hujianchen@suda.edu.cn

Background: The wide application of multi-walled carbon nanotubes (MWCNTs) in various fields has raised enormous concerns regarding their safety for humans. However, studies on the toxicity of MWCNTs to the eye are rare and potential molecular mechanisms are completely lacking. This study was to evaluate the adverse effects and toxic mechanisms of MWCNTs on human ocular cells.

Methods: Human retinal pigment epithelial cells (ARPE-19) were treated with pristine MWCNTs (7–11 nm) (0, 25, 50, 100 or 200 μg/mL) for 24 hours. MWCNTs uptake into ARPE-19 cells was examined using transmission electron microscopy (TEM). The cytotoxicity was evaluated by CCK-8 assay. The death cells were detected by Annexin V-FITC/PI assay. RNA profiles in MWCNT-exposed and non-exposed cells (n = 3) were analyzed using RNA-sequencing. The differentially expressed genes (DEGs) were identified through the DESeq2 method and hub of which were filtered by weighted gene co-expression, protein–protein interaction (PPI) and lncRNA-mRNA co-expression network analyses. The mRNA and protein expression levels of crucial genes were verified using quantitative polymerase chain reaction (qPCR), colorimetric analysis, ELISA and Western blotting. The toxicity and mechanisms of MWCNTs were also validated in human corneal epithelial cells (HCE-T).

Results: TEM analysis indicated the internalization of MWCNTs into ARPE-19 cells to cause cell damage. Compared with untreated ARPE-19 cells, those exposed to MWCNTs exhibited significantly decreased cell viabilities in a dose-dependent manner. The percentages of apoptotic (early, Annexin V positive; late, Annexin V and PI positive) and necrotic (PI positive) cells were significantly increased after exposure to IC50 concentration (100 μg/mL). A total of 703 genes were identified as DEGs; 254 and 56 of them were, respectively, included in darkorange2 and brown1 modules that were significantly associated with MWCNT exposure. Inflammation-related genes (including *CXCL8, MMP1, CASP3, FOS, CXCL2* and *IL11*) were screened as hub genes by calculating the topological characteristics of genes in the PPI network. Two dysregulated long non-coding RNAs (*LUCAT1* and *SCAT8*) were shown to regulate these inflammation-related genes in the co-expression network. The mRNA levels of all eight genes were confirmed to be upregulated, while caspase-3 activity and the release of CXCL8, MMP1, CXCL2, IL11 and FOS proteins were demonstrated to be increased in MWCNT-treated ARPE-19 cells. MWCNTs exposure also can induce cytotoxicity and increase the caspase-3 activity and the expression of LUCAT1, MMP1, CXCL2, and IL11 mRNA and protein in HCE-T cells.

Conclusion: Our study provides promising biomarkers for monitoring MWCNT-induced eye disorders and targets for developing preventive and therapeutic strategies.

Keywords: multi-walled carbon nanotubes, ocular toxicity, transcriptome, inflammation, apoptosis, long non-coding RNAs

Introduction

Carbon nanotubes (CNTs) are nano-sized one-dimensional tubular structures rolled by single (single-walled CNTs, SWCNTs) or multiple layers (multi-walled CNTs, MWCNTs) of graphene with unique electrochemical, mechanical and thermal properties, which render them as attracted engineered nanomaterials for various commercial applications.[1–4] An increase in the production and utilization of CNTs may result in their continuous exposure to occupational workers as well as consumers; thus, this may unavoidably induce potential human health risks. The

Received: 24 October 2022
Accepted: 6 May 2023
Published: 10 May 2023

human eyes are one of the superficial organs that could be directly exposed to airborne CNTs.[5] Although the eyeball has anatomical barriers to prevent the entry of foreign materials, this protection effect is limited to the large-sized airborne particles that could be excluded from the ocular surface by blinking and tear film. Nano-sized particles firmly attach to the cornea, penetrate the barriers of the ocular surface and reach the posterior segments of the eyes.[5] Once entering the eyes, nano-sized particles may subsequently induce toxicity on various ocular cells (eg, cornea, conjunctiva, lens, retina) and ultimately lead to the development of ocular diseases.[5–7] CNTs may also be accumulated in eyes as scaffolds,[8] electrodes of retinal implants,[9] drug delivery[10] and antibacterial agents[11,12] during the treatment of ocular diseases. Furthermore, CNTs may be orally or intravenously injected, lung-inhaled, and skin-absorbed followed by circulating in the bloodstream and then translocating to various organs (including eye in addition to frequently studied liver, kidneys, brain, et al).[13] More importantly, eye injuries and consequent blindness seriously impair peoples' quality of life. Therefore, the potential toxicity of CNTs on the eyes has been an issue which should be paid more attention by scientists and ophthalmologists.[5]

Currently, there were some in vitro and in vivo studies to demonstrate the toxicity of CNTs to the eyes. Yan et al used the human retinal pigment epithelial cell line (ARPE-19) as a model to evaluate the ocular toxicity of SWCNTs and MWCNTs. The results showed that both of SWCNT (diameter <2 nm)[14] and MWCNT (diameter of 10–30 nm)[15] exposure (especially unfunctionalized at 50 and 100 μg/mL) could significantly decrease the cell viability, elevate the lactate dehydrogenase level, increase the generation of reactive oxygen species (ROS) and induce some apoptosis or necrosis of ARPE-19 cells. Kishore et al injected MWCNTs into the conjunctival sac of left eyes of model rabbits and found that compared with the control right eyes, the treated left eyes exhibited conjunctival redness and discharge, with the Draize scoring for ocular lesions of 4.0 ± 0.00 (MWCNT1, diameter of 140 ± 30 nm) and 4.7 ± 1.15 (MWCNT2, diameter of 10–15 nm).[16] Exposure to water-dispersible SWCNTs was also observed to reduce the eye diameter of medaka embryos.[17] However, the studies focusing on the ocular toxicity effects of CNT exposure remain rare and underlying molecular mechanisms are completely unknown.

In the present study, we attempted to further explore the influence of MWCNTs (with smaller diameters than that of the study of Yan et al)[15] on the cell viability and apoptosis of ARPE-19 cells and, for the first time, investigate the molecular mechanisms underlying these toxicities by transcriptome sequencing (RNA-seq), bioinformatics analysis and wet experiment confirmation. RPE at the outer layer of the retina represents a crucial monolayer cell for maintaining the proper visual function by transporting nutrients from the choroidal capillary layer to the photoreceptor (which is a specialized type of neuron to absorb and convert light into electrophysiological signals for vision).[18] Thus, ARPE-19, an easy accessible and cost-effective cell line, was selected as an ocular cell model to examine the terminal visual toxicity of MWCNTs. Furthermore, cornea is located in the outermost surface of eyeball and may preferentially contact the MWCNTs and suffer damage.[5] Hereby, human corneal epithelial cell line (HCE-T) was also chosen as an in vitro experimental model to validate the ocular toxicity of MWCNTs, which was not reported previously. Our study may provide potential biomarkers for monitoring MWCNT-induced eye disorders and targets for developing preventive and therapeutic strategies.

Materials and Methods

Preparation of Dispersed MWCNTs

MWCNT powders were purchased from Jiangsu Cnano Technology Co., Ltd (Zhenjiang, Jiangsu, China). MWCNTs were not functionalized and retained their physiochemical properties as provided by the supplier: outer diameter, 7–11 nm; length, 5–20 μm; purity, 99.9%; BET special surface area, 200–300 m^2/g. The morphology of MWCNTs was further characterized by using transmission electron microscopy (TEM) in our study. MWCNT powders were dispersed in phosphate buffer solution (PBS) and sonicated for 10 minutes using an ultrasonic sample processing system LC-UP-400 (LICHEN, Shanghai, China) to prepare the stock solution (2 mg/mL).

Cell Culture

The human retinal pigment epithelial cell line ARPE-19 was purchased from National Collection of Authenticated Cell Cultures (Shanghai, China). ARPE-19 cells were cultured in Dulbecco's modified Eagle medium: Nutrient Mixture F12

(1:1) medium (DMEM/F12; Solarbio, Beijing, China) supplemented with 10% fetal bovine serum (FBS; Gibco, Grand Island, NY) and 1% (v/v) penicillin/streptomycin (Solarbio, Beijing, China). The human corneal epithelial cell line HCE-T was purchased from Fu Heng Biology (Shanghai, China). HCE-T cells were grown in DMEM/HamF12 medium plus 15% FBS, 5 μg/mL insulin and 10 ng/mL human epidermal growth factor (Fu Heng Biology, Shanghai, China). Both cells were maintained at 37°C in a humidified 5% CO_2 atmosphere and were harvested when they reached 80% confluency.

Cell Viability Assay

The effects of MWCNTs on the cell viability were determined by using a cell counting kit-8 (CCK-8; Beyotime, Shanghai, China). Briefly, ARPE-19 cells were seeded into 96-well plates at a density of 1.5×10^3 cells per well. After being adhered, the cells were treated with various concentrations of MWCNTs (0, 25, 50, 100 and 200 μg/mL), with five multiple wells set for each concentration. Following exposure to MWCNTs for 24 hours, 10 μL of CCK-8 solution was added into each well and the plates were incubated for another 4 hours. The absorbance was measured at 450 nm by using a microplate reader (Multiskan MK3, Thermo Scientific, MA, USA). The cell viability was expressed as percentage of untreated cells (100%) and then the 50% inhibitory concentration (IC50) was calculated.

Cell Death Assay

The effects of MWCNTs on the cell apoptosis were examined by using the Annexin V-fluorescein isothiocyanate (FITC)/propidium iodide (PI) apoptosis kit (4A Biotech Co., Ltd, Beijing, China). Briefly, ARPE-19 cells were exposed to MWCNTs at concentrations corresponding to 0 μg/mL and IC50 for 24 hours. The floating and adherent ARPE-19 cells were collected and washed twice with cold phosphate-buffered saline. Cell pellets were re-suspended in 500 μL of 1 × binding buffer and incubated with 5 μL Annexin V-FITC and 5 μL PI for 15 minutes at room temperature in the dark. The apoptotic [the sum of early apoptosis (right-lower quadrant; Annexin V+/PI-) and late apoptosis (right-upper quadrant; Annexin V+/PI+)] and necrotic (left-upper quadrant; Annexin V-/PI+) rates of ARPE-19 cells were detected by using CytoFLEX flow cytometer (Beckman Coulter, California, USA). Experiments were run in triplicate.

Determination of Intracellular Location of MWCNTs

TEM was used to indicate the internalization of MWCNTs and ultrastructural pathologic changes in ARPE-19 cells. Following exposure to MWCNTs for 24 hours, the ARPE-19 cells were harvested and washed with PBS for three times. After centrifugation at 1000 rpm for 5 minutes to remove the supernatant, the cells were fixed in 3% glutaraldehyde overnight, post-fixed in 1% osmium tetroxide for 2 hours, dehydrated with increasing concentrations of ethanol (30%, 50%, 70%, 80%, 95% and 100%) and embedded in epoxy resin (Epon 812). Ultra-thin sections (approximately 60–80 nm) were cut using an ultramicrotome (LEICA UC7, Germany) with a diamond knife, mounted on 150 mesh copper grids and post-stained with 2% uranyl acetate and 2.6% lead citrate. Thin sections were observed under a TEM (HT7800, Hitachi High-Tech, Hitachinaka-shi, Japan) operated at an operating voltage of 80 kV.

Next-Generation RNA Sequencing (RNA-Seq) Analysis

ARPE-19 cells were incubated with IC50 concentrations of MWCNTs for 24 hours. Total RNA was extracted from control or MWCNT-treated cells by using the Trizol reagent (Invitrogen, Carlsbad, CA, USA) and RNeasy MinElute spin columns (Qiagen, Valencia, CA, USA). The integrity of the total RNA was determined by Agilent 2100 Bioanalyser (Agilent Technologies, Santa Clara, CA, USA). The quantification of the total RNA was performed using the spectrophotometer NanoDrop2000 (Thermo Scientific, Waltham, MA, USA). About 500 ng of high-quality RNA samples ($OD_{260/280}$ = 1.9–2.0, RNA integrity number ≥8) was used to construct the sequencing library. The libraries were prepared and sequenced by Mingma Technology (Shanghai, China). The sequencing was run on the Illumina NovaSeq 6000 platform (Illumina, San Diego, CA, USA) with a paired-end read length of 150 bp.

Bioinformatics Analysis

The qualities of raw reads from six samples were checked using FASTQC software (v0.11.9; https://www.bioinformatics.babraham.ac.uk/projects/fastqc/). Adapter- and quality-trimming were performed by using Trim galore software (v0.6.7; https://www.bioinformatics.babraham.ac.uk/projects/trim_galore/). The clean reads were aligned to the Ensembl GRCh38 reference genome by using the STAR aligner (v2.7.10a; https://github.com/alexdobin/STAR).[19] The number of reads mapped to each gene was counted with HTSeq-count (v12.3; https://htseq.readthedocs.io/en/master/htseqcount.html).[20]

The genes with read count values < 1 in more than three samples were filtered. The read counts were normalized for library size differences using "estimateSizeFactorsForMatrix" function from DESeq2 package (v1.36.0, https://bioconductor.org/packages/release/bioc/html/DESeq2.html).[21] Differentially expressed genes [DEGs; including various RNA types, such as messenger RNAs (DE-mRNAs), long non-coding RNAs (DE-lncRNAs) and others] between MWCNT-treated and control ARPE-19 cells were identified using the DESeq2 package with the "nbinomWaldTest" function. The thresholds for significant differential expression were set as Benjamini-Hochberg false discovery rate (FDR) < 0.01 and $|\log_2$fold change (FC)| > 1. The volcano plot and heatmap of DEGs were plotted by using the "ggplot2" (v3.3.6; https://cran.r-project.org/web/packages/ggplot2/) and "pheatmap" package (v1.0.8; https://cran.r-project.org/web/packages/pheatmap), respectively.

The weighted gene co-expression network analysis (WGCNA) is an algorithm that can cluster highly correlated genes into co-expressed modules and discover modules significantly associated with disease phenotypes.[22] Thus, WGCNA package in R (v1.61; https://cran.r-project.org/web/packages/WGCNA/index.html)[22] was used to identify modules associated with MWCNT-induced toxicity in ARPE-19 cells. The optimal soft threshold power (β) was selected using the function of "pickSoftThreshold" according to the principle of scale-free topology network. The adjacency matrix was transformed into a topological overlap matrix (TOM) and the corresponding dissimilarity (1-TOM) was used to construct a hierarchical clustering dendrogram. The dynamic tree cut algorithm was used to extract gene modules with a minimum module size of 50, unmerged cut height of 0.995, merged cut height of 0.25 and deep split of 1. Module-trait relationships were calculated by Pearson's correlation tests to assess the correlation between module eigengenes (MEs, representing the overall expression level of the gene module) and MWCNT-induced phenotypes. The gene significance (GS, representing the association of individual genes with that trait), module membership (MM, representing the correlation of gene expression profile with MEs) and their correlations were also computed. Additionally, differentially expressed genes were mapped into the modules by using the hypergeometric algorithm [f (k, N, M, n) = C (k, M)*C (n-k, N-M)/C (n, N)]. The modules were considered to be particularly relevant to MWCNT exposure if they met the criteria: 1) significantly associated with traits ($p < 0.05$); 2) there were significant associations between GS and MM ($p < 0.05$); 3) significantly enriched with DEGs ($p < 0.05$ and enrichment fold >1). In key modules, the enriched DEGs that had the higher absolute value of GS and MM (>0.6) were considered to be important genes.

To further mine hub DE-mRNAs, the interaction relationships among the DEGs were predicted by the Search Tool for the Retrieval of Interaction Genes (STRING; v10.0; http://stringdb.org/) database.[23] The relationship pairs with a combined score ≥0.4 were retained to construct the protein–protein interaction (PPI) network. The hub genes were identified by calculating their topological characteristics (including degree, betweenness and closeness) by using the CytoNCA plugin in the Cytoscape software (http://apps.cytoscape.org/apps/cytonca).[24] The genes ranked in the top 30 of these three topological characteristics were suggested as hub genes. Furthermore, significant clustering modules (MCODE score >6 and the number of nodes >4) were also detected from the PPI network using the Molecular Complex Detection (MCODE; v1.4.2, http://apps.cytoscape.org/apps/mcode) plugin in the Cytoscape software.[25] The hub genes included in modules were regarded crucial.

To understand potential functions of hub DE-mRNAs, Gene Ontology (GO) and Kyoto Encyclopedia of Genes and Genomes (KEGG) pathway analyses were performed by using the Database for Annotation, Visualization and Integrated Discovery (DAVID) (v6.8; http://david.abcc.ncifcrf.gov). $P < 0.05$ was set as the cutoff criterion. The "Goplot2" package in R was used to generate the chord plot for hub DE-mRNAs.

To reveal the regulatory mechanisms of DE-lncRNAs, a co-expression network between DE-lncRNAs and hub DE-mRNAs was constructed by calculating their Pearson correlation coefficients (PCCs). PCC > 0.9 and p-value <0.01 were defined as the thresholds for meaningful correlation. The co-expression network was visualized by using Cytoscape (v3.6.1; www.cytoscape.org/).

Quantitative Real-Time Polymerase Chain Reaction (qRT-PCR) Analysis

qRT-PCR was used to validate the mRNA expression levels of crucial genes. After ARPE-19 cells were exposed to IC50 concentrations of MWCNTs or control for 24 hours, total RNA was extracted by using the Trizol reagent (Invitrogen). Then, the total RNA (2 μg per 40 μL reaction) was reverse-transcribed into cDNA using the M-MLV reverse transcriptase (Invitrogen). qRT-PCR reactions were performed on the LightCycler 480II Real-Time PCR System (Roche Diagnostics, Basel, Switzerland) by using TB Green® Premix Ex Taq™ II (Tli RNaseH Plus) (Takara, Dalian, China). The PCR cycle was as follows: 95°C for 5 minutes, 40 cycles of 95°C for 10 seconds and 60°C for 15 seconds, followed by 60°C to 95°C melting curve detection. Primers were synthesized by the Tianyihuiyuan Biotechnology Co., Ltd (Beijing, China) and listed in Table 1. The relative expression levels of genes were calculated using the $2^{-\Delta\Delta Ct}$ method after normalization to endogenous control β-actin. Experiments were run in triplicate and repeated three times for each sample.

Caspase-3 Activity Assay

The caspase-3 enzymatic activity was determined by using the Caspase-3 colorimetric assay kit according to the manufacturer's instruction (Beyotime, Shanghai, China). Briefly, the ARPE-19 and HCE-T cells treated with indicated concentrations of MWCNTs for 24 hours were washed three times with PBS and lysed with lysis buffer for 15 minutes. After centrifugation at 4000 rpm for 20 minutes, the cell supernatant was treated with the caspase-3 substrate Ac-DEVD-pNA and incubated at 37°C for 2 hours. The absorbance of the released pNA was then measured using an ELISA plate reader (BK-EL10C, BIOBASE, Jinan, China) at 405 nm and the concentrations of pNA were plotted according to the standard curve. Experiments were run in triplicate.

Enzyme-Linked Immunosorbent Assay (ELISA)

The supernatants of ARPE-19 and HCE-T cells treated with indicated concentrations of MWCNTs for 24 hours were collected after centrifugation at 4000 rpm for 20 minutes. The release of C-X-C motif chemokine ligand 8 (CXCL8), C-X-C motif chemokine ligand 2 (CXCL2), interleukin 11 (IL11) and matrix metallopeptidase 1 (MMP1) proteins was measured by using corresponding ELISA kits according to the manufacturer's instruction (Ruixin Biology, Quanzhou,

Table 1 Primer Sequences of Crucial Genes

Gene Name	Accession Number in NCBI	Primer Sequences (5'to3')	Length, bp
MIR4280HG	117751736	Forward: GGCATCACGCTACCTGACTTCAA Reverse: CGGCATTATTTCTGAGGGCTCTGT	123
SCAT8	112935969	Forward: GTAGTGTACTGACTTCTGCCTGGA Reverse: GCCTCTGGAGTGCTGAACAATTC	117
LUCAT1	100505994	Forward: GGCTACATGCTGAGCTACAGAGTT Reverse: GAGGCAGGAGAATGGCGTGAAC	114
FOS	2353	Forward: CCGAGATTGCCAACCTGCTGAA Reverse: TCCATGCTGCTGATGCTCTTGAC	247
CASP3	836	Forward: AGAGACATGACTCAGCCTGTTCCA Reverse: GGCAGCATCATCCACACATACCA	105
CXCL8	3576	Forward: CTGAGAGTGATTGAGAGTGGACCA Reverse: ACTGGCATCTTCACTGATTCTTGG	193
IL11	3589	Forward: GGACTGCTGCTGCTGAAGACTC Reverse: GCCTCACGGAAGGACTGTCTCTA	166
CXCL2	2920	Forward: ACCGAAGTCATAGCCACACTCAAG Reverse: CTTCAGGAACAGCCACCAATAAGC	152
MMP1	4312	Forward: CCAGATGTGGAGTGCCTGATGTG Reverse: CCTTGGTGAATGTCAGAGGTGTGA	186
β-actin	60	Forward: TCCATCATGAAGTGTGACGT Reverse: GAGCAATGATCTTGATCTTCAT	154

China). Optical densities were read by using an ELISA plate reader (BK-EL10C, BIOBASE, Jinan, China) at 450 nm and the concentrations of each protein were plotted according to the standard curve. Experiments were run in triplicate.

Western Blotting

ARPE-19 and HCE-T cells treated with indicated concentrations of MWCNTs for 24 hours were lysed with ice-cold RIPA lysis buffer (Solarbio Science & Technology Co., Ltd, Beijing, China) to extract the total proteins. Protein concentration was measured using the BCA Protein Assay Kit (Solarbio Science & Technology Co., Ltd, Beijing, China). Equal amounts of protein (30 μg) were separated on 10% sodium dodecylsulfate polyacrylamide gel electrophoresis and then transferred to a polyvinylidene difluoride membrane (Millipore, Billerica, MA, USA). Membranes were blocked with 5% skimmed milk at room temperature for one hour and afterward probed with a primary antibody against Fos proto-oncogene, AP-1 transcription factor subunit (FOS) (ProteinTech, Chicago, IL, USA; diluted 1:5000) and β-tubulin (Abcam, Cambridge, UK; diluted 1:2000) overnight at 4°C. After being washed, the membranes were then incubated with horseradish peroxidase-conjugated secondary antibodies (EarthOx Life Sciences, San Francisco, CA, USA) at room temperature for one hour. Protein bands were visualized using an enhanced chemiluminescence (ECL) kit (Beyotime, Shanghai, China). The blots were scanned and the band intensity was quantified using ImageJ software (v1.48; National Institutes of Health, Bethesda, MD, USA). β-tubulin was used as the reference control. Experiments were run in triplicate.

Statistical Analysis

All experimental data were presented as means ± standard deviation. IC50 value of the cytotoxicity assay was calculated by non-linear regression analysis [Dose-response-Inhibition, log (inhibitor) vs normalized response-variable slope] using GraphPad Prism 5.0 software (San Diego, CA, USA). Statistical analyses were performed by SPSS 16.0 software (Chicago, IL, USA). The data of the cell viability were analyzed using one-way ANOVA with Dunnett's post hoc test. The data of apoptosis, qRT-PCR, ELISA, caspase-3 activity and Western blotting were analyzed using a paired *t*-test. Two-sided p-values < 0.05 were considered statistically significant.

Results

Characteristics of MWCNTs

TEM analysis was performed for MWCNTs that were suspended in PBS and sonicated for 10 minutes. As shown in Figure 1A and B, the MWCNTs samples exhibited a tangled, hollow shape and the presence of multiple well-arranged graphene sheets. The diameters of MWCNTs were not changed after sonication (still within 10 nm).

MWCNT Exposure Reduces the Viability in ARPE-19 Cells

The cytotoxicity of MWCNTs on ARPE-19 cells was determined by the CCK-8 cell viability assay. As shown in Figure 2A, MWCNTs induced the decline of ARPE-19 cell viability in a concentration-dependent manner. Compared with untreated controls, a significant decrease in the viability of ARPE-19 cells was observed from the MWCNT concentration of 50 μg/mL (Figure 2A). By using a non-linear regression curve fitting analysis in the GraphPad Prism software, the IC50 value was calculated as 100.2 μg/mL (Figure 2B). Thus, this concentration was used for the following studies.

MWCNT Exposure Induces Death in ARPE-19 Cells

To assess whether the cytotoxicity of MWCNTs on ARPE-19 cells resulted from cell death, Annexin V-FITC/PI staining and flow cytometry assay were performed. Our results showed that the percentages of total (including early and late) apoptotic cells (11.3 ± 1.3% vs 4.1 ± 0.6%, $p = 0.004$) and necrotic cells (11.4 ± 0.5% vs 1.0 ± 0.4%, $p = 0.002$) were significantly increased in ARPE-19 cells exposed to MWCNTs relative to untreated control cells (Figure 2C and D).

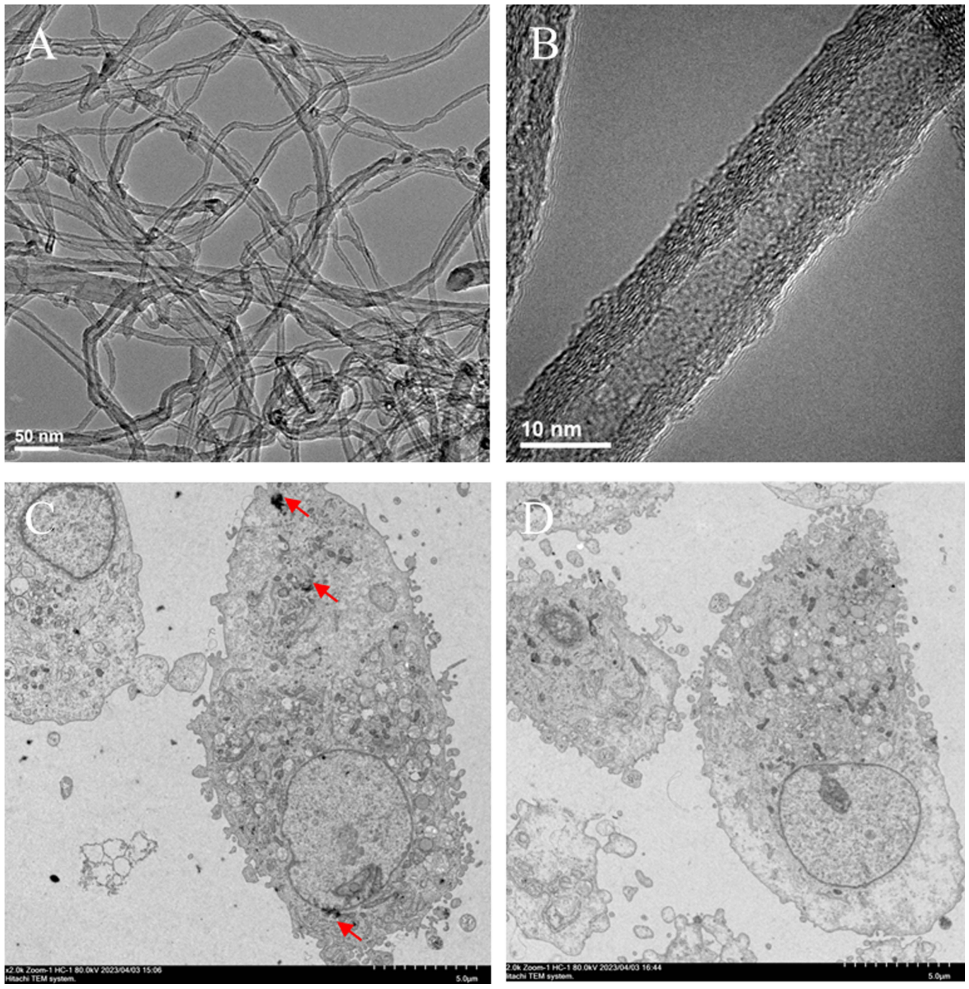

Figure 1 Transmission electron microscopy analysis. (**A** and **B**): the morphology of MWCNTs. Scale bar: 50 nm (**A**), 10 nm (**B** and **C**): the internalization of MWCNTs (arrow) into human retinal pigment epithelial ARPE-19 cells. Magnification, × 2000. Scale bar: 5 μm; (**D**), the morphology of human retinal pigment epithelial ARPE-19 cells without exposed to MWCNTs. Magnification, × 2000. Scale bar: 5 μm.
Abbreviation: MWCNTs, multi-walled carbon nanotubes.

Internalization of MWCNTs and Ultrastructural Changes of ARPE-19

TEM assay revealed the internalization of MWCNTs inside the ARPE-19 cells with a primary localization in the cytoplasm and nucleus (Figure 1C). Compared with normal morphologies in the non-exposed control cells (Figure 1D), MWCNT exposed ARPE-19 cells exhibited obvious damage or disappearance of the organelles (eg, mitochondria) (Figure 1C) which has been recognized as a key factor to trigger cell death signaling.[26,27]

Transcriptome Analysis Identifies Hub Genes Associated with MWCNT-Induced Toxicity in ARPE-19 Cells

Identification of DEGs

After preprocessing, an expression matrix containing 25,022 genes was obtained. Differential expression analysis was then performed for them by the DESeq2 software. Under the strict criteria of FDR < 0.01 and $|\log_2 FC| > 1$, 703 DEGs were identified between MWCNT-treated and untreated control ARPE-19 cells, including 261 upregulated (gene type: mRNAs, n = 212; lncRNAs, n = 42; pseudogenes, n = 6; TEC, n = 1) and 442 downregulated (gene type: mRNAs, n = 266; lncRNAs, n = 139; pseudogenes, n = 27; TEC, n = 7; microRNA, n = 1; misc_RNA, n = 2) (Figure 3A). The heat map illustrated that MWCNT-treated cell samples were obviously discriminated from untreated controls by the expression levels of these 703 DEGs (Figure 3B).

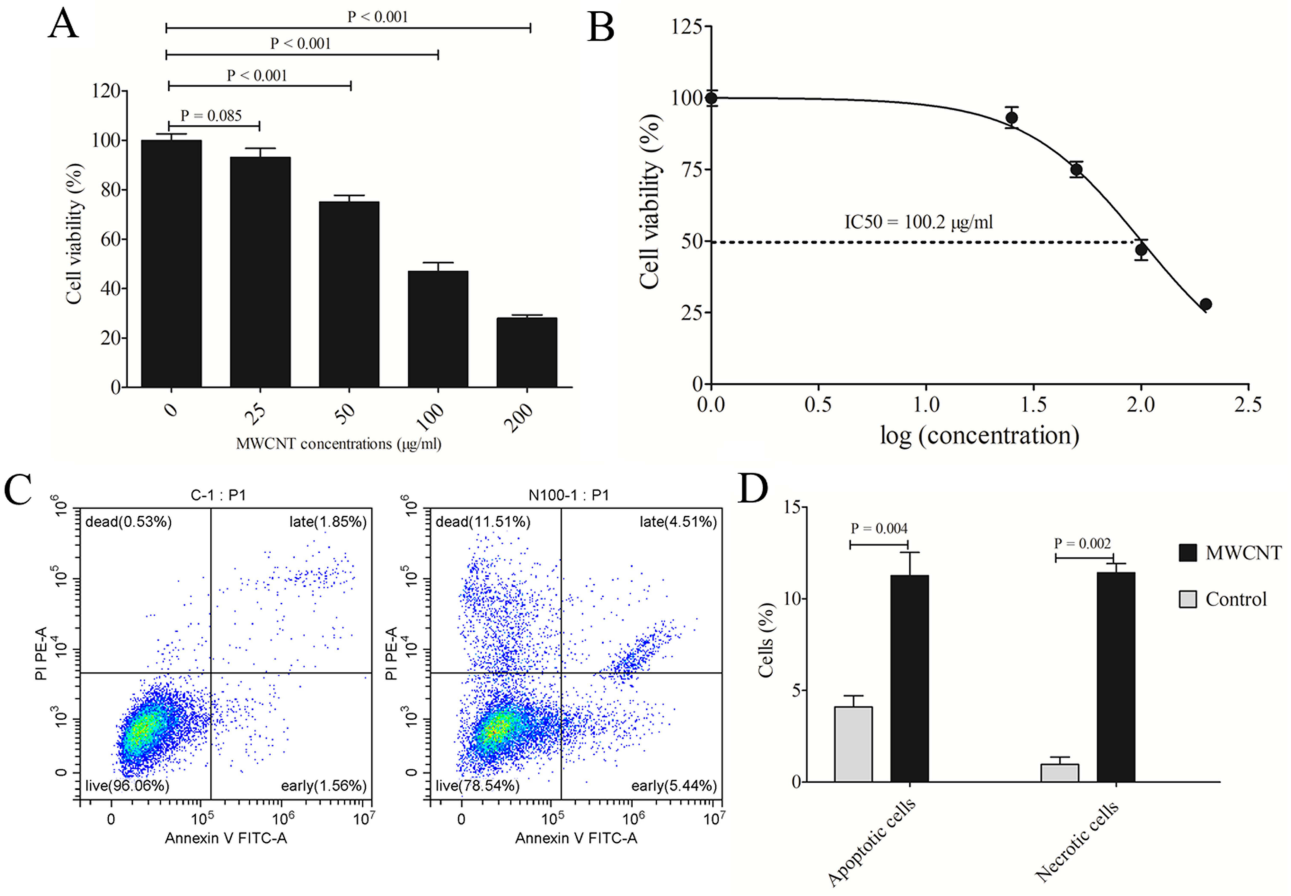

Figure 2 MWCNT-induced toxicities on human retinal pigment epithelial ARPE-19 cells. (**A**), cell viability analysis after 24 hours of exposure to different concentrations of MWCNTs (0–200 μg/mL); (**B**), determination of IC50 values; (**C**), cell apoptosis analysis after 24 hours of exposure to concentrations corresponding to 0 μg/mL (left, C-1) and IC50 (100 μg/mL; right, N-100-1) of MWCNTs; (**D**), bar graphs to show the percentages of apoptotic and necrotic cells.
Abbreviations: MWCNTs, multi-walled carbon nanotubes; IC, inhibitory concentration.

Identification of Key Modules Associated with MWCNT Exposure

All 25,022 genes were used to build the co-expression modules using WGCNA. The soft-threshold power was selected as 24 (scale free $R^2 = 0.89$ and the lower level of average connectivity) to construct a scale-free network (Figure 4). After merging similar modules, 36 modules were identified (Figure 5A), with the module size presented in Table 2. The module-trait relationship heatmap indicated only three modules were strongly correlated with MWCNT-induced phenotypes (darkorange2 module: r = 0.89, p = 0.02; brown1 module: r = −0.86, p = 0.03; darkolivegreen1 module: r = −0.87, p = 0.03; Figure 5B). Of them, darkorange2 (mRNAs, n = 209; lncRNAs, n = 38; pseudogenes, n = 6; TEC, n = 1) and brown1 modules (mRNAs, n = 25; lncRNAs, n = 24; pseudogenes, n = 6; misc_RNA, n = 1) were significantly enriched by 254 and 56 DEGs, respectively (Table 2 and Table S1). There were significant correlations between GS for the disease status and MM in the brown1 (Figure 5C) and darkorange2 (Figure 5D) modules. Also, the |GS| and |MM| of all these genes were more than 0.6. These findings suggested these two modules and their included DEGs were crucial for MWCNT-induced toxicity in ARPE-19 cells.

Identification of Hub DE-mRNAs in Two Key Modules

A total of 234 DE-mRNAs enriched in the above two key modules were uploaded into the STRING database to obtain the interaction relationship pairs. As a result, 474 interaction pairs among 164 genes (such as *FOS-CASP*3, *FOS- IL11*/*CXCL8*/*CXCL2, CXCL8-CASP3, CXCL8*/*IL11*/*CXCL2-MMP1, MMP1-CASP3*; Table S2) were predicted, which were used to construct the PPI network. After calculation of three topological characteristics (degree, betweenness and closeness) for each node in the PPI network, 50 genes were found to be ranked in the top 30 (Table 3). Subsequent MCODE analysis extracted two function-related modules from the PPI network (Figure 6), in which 23 (*IL33*, interleukin

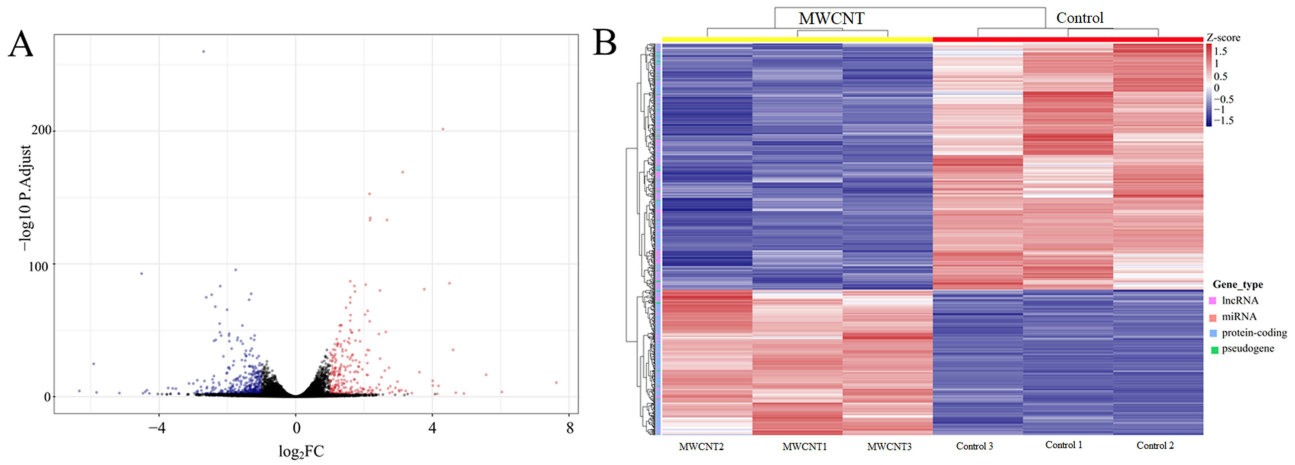

Figure 3 Identification of differentially expressed genes. (**A**), volcano plot of differentially expressed genes between MWCNT-treated and control cells (red, upregulated; blue, downregulated; black, non-significant); (**B**), heat map analysis of differentially expressed genes between MWCNT-treated and control cells (red, upregulated; blue, downregulated).
Abbreviations: MWCNTs, multi-walled carbon nanotubes; FC, fold change.

33; *PLAT*, plasminogen activator, tissue type; *CXCL8; FOS; CXCL2; RELB*, RELB proto-oncogene, NF-kB subunit; *CXCL1*, C-X-C motif chemokine ligand 1; *FOSB*, FosB proto-oncogene, AP-1 transcription factor subunit; *CD274; TNFAIP3*, TNF alpha induced protein 3; *ICAM1*, intercellular adhesion molecule 1; *CASP3*, caspase 3; *FOSL*1, FOS like 1, AP-1 transcription factor subunit; *TRAF1*, TNF receptor associated factor 1; *VEGFC*, vascular endothelial growth factor C; *IL1RN*, interleukin 1 receptor antagonist; *TNFRSF11B*, TNF receptor superfamily member 11b; *CSF2*, colony stimulating factor 2; *MMP1; CCRL2*, C-C motif chemokine receptor like 2; *NR4A1*, nuclear receptor subfamily 4 group A member 1; *IL11; PLAUR*, plasminogen activator, urokinase receptor) were overlapped with the above 50 genes. These findings implied these 23 DE-mRNAs were potential hub DE-mRNAs for MWCNT-induced toxicity in ARPE-19 cells.

Function Enrichment for Hub DE-mRNAs

The 234 DE-mRNAs enriched in key modules were uploaded into the DAVID database to predict their possible functions. The results showed 114 GO biological process items and 17 KEGG pathways were significantly enriched (Table S3). The hub genes were found to be mainly involved in inflammation-, proliferation- and apoptosis-related function results, such as GO:0006955~immune response (p = 1.07E-04; *CXCL8, CXCL2*), GO:0006954~inflammatory response (p = 1.95E-04; *CXCL8, FOS, CXCL2*), GO:0043065~positive regulation of apoptotic process (p = 4.14E-03; *CASP3*), GO:0008285~negative regulation of cell proliferation (p = 3.41E-02; *CXCL8*), hsa04668:TNF signaling pathway (p = 1.39E-06; *CASP3, FOS, CXCL2*), hsa04657:IL-17 signaling pathway (p = 2.06E-06; *CXCL8, MMP1, CASP3, FOS, CXCL2*), hsa04060:Cytokine-cytokine receptor interaction (p = 1.55E-05; *IL11, CXCL8, CXCL2*) and hsa04064: NF-kappa B signaling pathway (p = 3.67E-05; *CXCL8, CXCL2*) (Figure 7).

Identification of Hub DE-lncRNAs in Two Key Modules

To further identify hub DE-lncRNAs and predict underlying function mechanisms, co-expression relationships between 62 DE-lncRNAs in two key modules and 23 hub DE-mRNAs were calculated. According to the thresholds of PCC > 0.9 and p-value <0.01, 504 co-expression relationship pairs were predicted between 52 DE-lncRNAs and inflammation-, proliferation- and apoptosis-related DE-mRNAs, such as *MIR4280HG-CXCL2/CASP3/CXCL8/IL11/MMP1/FOS, LUCAT1-FOS/MMP1/CXCL2/CXCL8/IL11* and *SCAT8 -MMP1/CXCL8/CASP3/CXCL2/FOS/IL11* (Figure 8).

Validation of Hub DE-lncRNAs and DE-mRNAs in ARPE-19 Cells

qRT-PCR was performed to validate the expression levels of hub DE-lncRNAs and DE-mRNAs in MWCNT-exposed ARPE-19 cells and controls. The results showed that the expression levels of *SCAT8, LUCAT1, FOS, CASP3, CXCL8, IL-11, CXCL2* and *MMP1* were consistent between RNA-seq (Figure 9A) and qRT-PCR (Figure 9B) experiments, all of which were significantly increased in MWCNT-exposed ARPE-19 cells in contrast to untreated control cells.

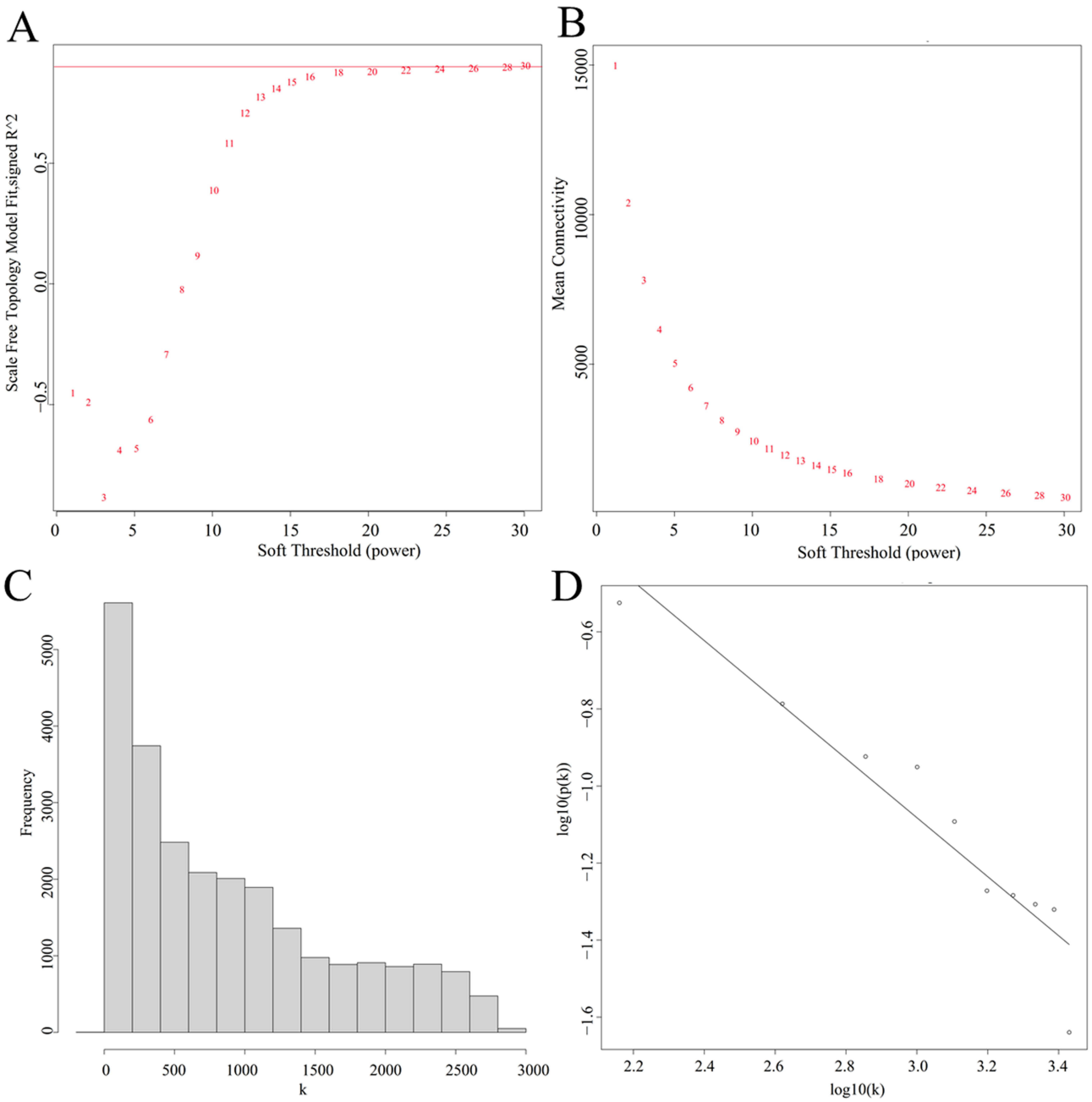

Figure 4 Determination of the optimal soft-thresholding power in WGCNA. (**A**), analysis of the scale-free fit index for various soft-thresholding powers (β); (**B**), analysis of the mean connectivity for various soft-thresholding powers; (**C**), histogram of the connection distribution when β was 24; (**D**), checking the scale-free topology when β was 24. Scale R^2 = 0.89, slope = −0.77.

Abbreviation: WGCNA, weighted gene co-expression network analysis.

MIR4280HG was found not to be significantly changed in qRT-PCR validation experiments (Figure 9B). Furthermore, the protein expression levels of DE-mRNAs were also examined by ELISA, caspase-3 activity assay and Western blotting. As expected, we confirmed the production of CXCL8, MMP1, CXCL2, IL11 (Figure 9C), the caspase-3 activity (Figure 9D) and FOS protein expression (Figure 9E and F) were all significantly increased in MWCNT-treated ARPE-19 cells in comparison with the control cells.

Validation of the Toxicity and Mechanisms of MWCNTs in HCE-T Cells

Exposure of HCE-T cells to 100 μg/mL MWCNTs could cause the cell viability decline to 66.02 ± 2.84% of the control (Figure 10A). qRT-PCR analysis showed the significant up-regulation of *LUCAT1, IL-11, CXCL2* and *MMP1* in HCE-T cells

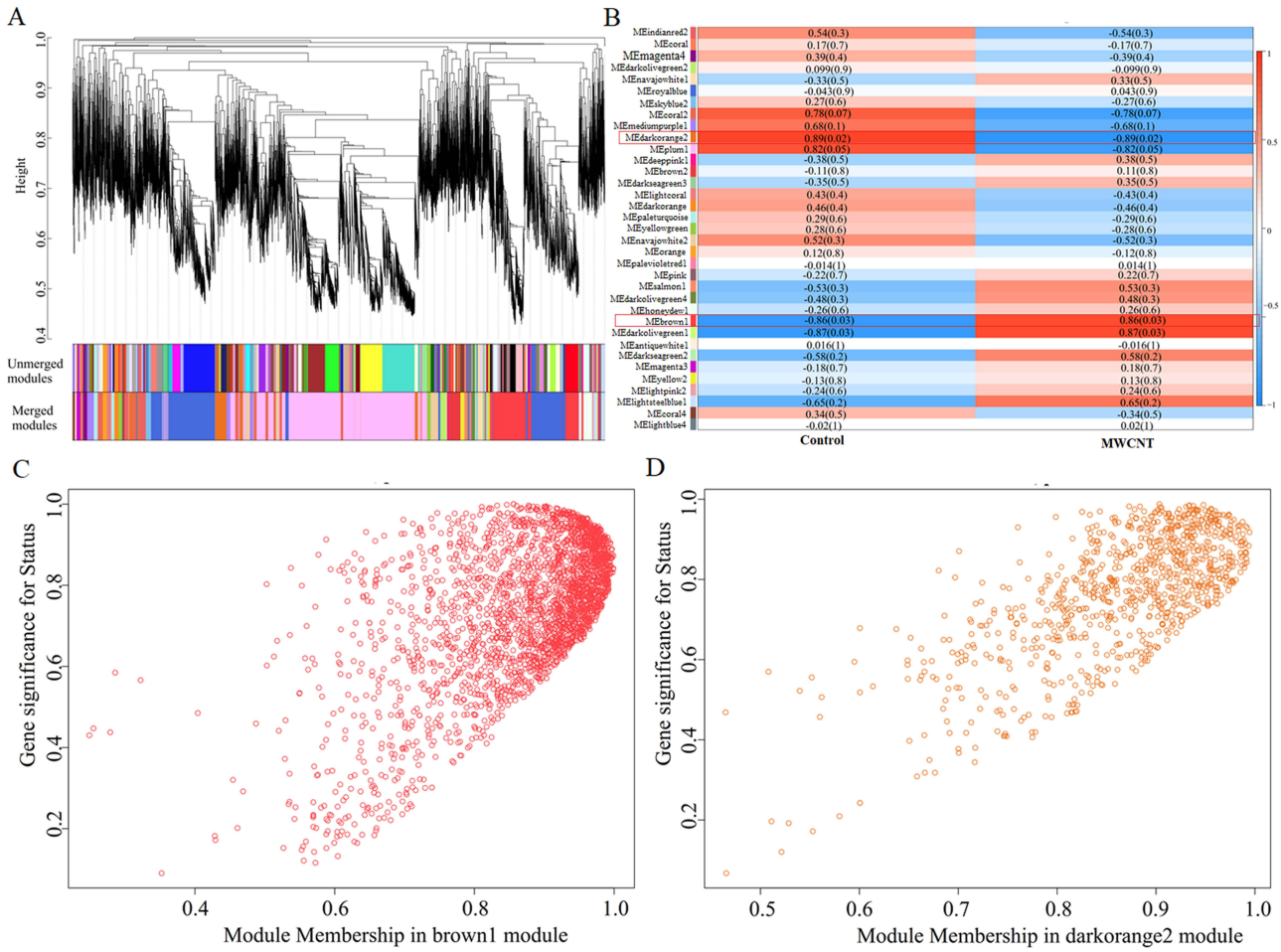

Figure 5 Identification of crucial co-expressed modules associated with MWCNT-induced toxicity in ARPE-19 cells. (**A**), the clustering dendrogram. Different colors were assigned to corresponding modules. Branches above indicate genes and different colors below represent specific co-expression modules; (**B**), Module-trait correlations. Each row corresponds to a module eigengene (ME) and each column corresponds to a phenotype. Each cell includes the correlation coefficient and p-value (in bracket). Red box indicates modules significantly associated with MWCNT treatment; (**C**), correlation between module membership of brown 1 module and gene significance with clinical traits (cor = 0.61, p < 1E-200); (**D**), correlation between module membership of darkorange2 module and gene significance with clinical traits (cor = 0.71, p < 6.7E-150). **Abbreviation**: Cor, correlation coefficient.

after exposed to MWCNTs (Figure 10B). Colorimetric assay indicated the caspase-3 activity was significantly increased in HCE-T cells undergoing 24-hours incubation with MWCNTs (Figure 10C). ELISA demonstrated compared with the control cells, the release of MMP1, CXCL2 and IL11 was significantly higher in HCE-T cells at the 24-hour post-exposure of MWCNTs (Figure 10D). Unlike with ARPE-19 cells, we found the mRNA and protein expression levels of FOS were significantly reduced in MWCNT-treated HCE-T cells compared with the controls (Figure 10B, E and F). There were no significant differences in *MIR4280HG, SCAT8* and *CXCL8* between MWCNT-exposed and non-exposed HCE-T cells.

Discussion

The wide application of MWCNTs in various fields has raised enormous concerns regarding their health risks for humans. Although the toxicity of MWCNTs had been investigated by numerous studies, most of literatures explored the influence on the inner organs (such as lung,[28,29] liver, kidney,[30] brain[31] or reproductive systems).[32] The eye toxicity of MWCNTs was relatively ignored.[15,16] The current study was designed to further assess the toxicity of MWCNTs on retinal cell line ARPE-19. Our results showed that MWCNT exposure was able to reduce the viability of ARPE-19 cells in a dose-dependent manner and induce cell apoptosis and necrosis, which were similar to the conclusions obtained by Yan et al.[15] However, different from the study of Yan et al (72 hours of exposure),[15] our study found the viability of 50% cells were inhibited at the concentration of 100 μg/mL only after exposure for 24 hours. This result indicated the higher

Table 2 Modules Identified by WGCNA

ID	Module	Module Size	#DEGs	Enrichment Infor	
				Enrichment Fold[95% CI]	P_{hyper}
Module 1	Antiquewhite1	72	0	-	-
Module 2	Brown1	2619	254	5.36[4.55–6.3]	1.08E-77
Module 3	Brown2	556	0	-	-
Module 4	Coral	102	0	-	-
Module 5	Coral2	1340	27	0.72[0.47–1.06]	1.02E-01
Module 6	Coral4	187	0	-	-
Module 7	Darkolivegreen1	119	5	1.56[0.5–3.78]	2.63E-01
Module 8	Darkolivegreen2	261	0	-	-
Module 9	Darkolivegreen4	176	0	-	-
Module 10	Darkorange	193	0	-	-
Module 11	Darkorange2	972	56	2.27[1.68–3.02]	1.87E-07
Module 12	Darkseagreen2	169	1	0.21[0.01–1.19]	9.58E-02
Module 13	Darkseagreen3	104	0	-	-
Module 14	Deeppink1	136	0	-	-
Module 15	Grey	2	0	-	-
Module 16	Honeydew1	546	0	-	-
Module 17	Indianred2	439	0	-	-
Module 18	Lightblue4	145	0	-	-
Module 19	Lightcoral	212	0	-	-
Module 20	Lightpink2	80	0	-	-
Module 21	Lightsteelblue1	294	1	0.12[0–0.68]	5.78E-03
Module 22	Magenta3	194	0	-	-
Module 23	Magenta4	209	0	-	-
Module 24	Mediumpurple1	663	7	0.37[0.15–0.78]	5.04E-03
Module 25	Navajowhite1	250	0	-	-
Module 26	Navajowhite2	759	1	0.05[0–0.26]	2.33E-08
Module 27	Orange	195	0	-	-
Module 28	Paleturquoise	328	1	0.11[0–0.61]	1.87E-03
Module 29	Palevioletred1	168	0	-	-
Module 30	Pink4	97	0	-	-
Module 31	Plum1	7594	350	2.39[2.05–2.78]	6.04E-29
Module 32	Royalblue	4781	0	-	-
Module 33	Salmon1	151	0	-	-
Module 34	Skyblue2	300	0	-	-
Module 35	Yellow2	258	0	-	-
Module 36	Yellowgreen	351	0	-	-

Abbreviations: DEGs, differentially expressed genes; CI, confidence interval.

toxicity of our used MWCNTs (small diameter, 7–11 nm) relative to that of Yan et al (large diameter of 10–30 nm),[15] which conformed to diameter-dependent toxicity effects of MWCNTs identified in human umbilical vein endothelial cells.[33] Interestingly, different from our results, some previous studies of lung cells and tissues found opposite conclusions (that is, MWCNTs with a large diameter resulted in higher toxicity than MWCNTs with a small diameter).[34–36] On one hand, these findings imply the toxicity effects of MWCNTs may be cell- or tissue-specific, which may provide the theory for designing more suitable and biocompatible MWCNTs in the treatment of diseases targeting different organs; on the other hand, the controversial differences in diameter-dependent toxicity above can be explained by the fact that MWCNTs with a large diameter may be relatively difficult to be cleared in inner organs and the resulting injuries may be severe, while large-sized MWCNTs are easily blocked from the ocular surface by blinking and tear film[5] and thus, small-sized MWCNTs-induced injuries may be especially evident.[16] Furthermore, in the study of Yan et al,[15] cell apoptosis was

Table 3 Topological Characteristics for Genes in the Protein–Protein Interaction Network

Genes	Degree	Genes	Betweenness	Genes	Closeness
CXCL8	39	*FOS*	4212.811	*CXCL8*	0.041518
ICAM1	35	*CXCL8*	3484.123	*FOS*	0.041423
FOS	34	*CASP3*	2694.539	*ICAM1*	0.041371
CSF2	28	*SGK1*	2306.156	*CSF2*	0.041371
CXCL1	24	*NT5E*	2113.149	*CASP3*	0.041172
MMP1	22	*NEDD4L*	2079.475	*CXCL1*	0.041151
CASP3	21	*DDIT3*	1995.597	*EGR1*	0.04112
EGR1	18	*ICAM1*	1868.038	*DDIT3*	0.041006
CXCL2	18	*CSF2*	1715.732	*MMP1*	0.041006
FOSL1	16	*EGR1*	1585.743	*FOSL1*	0.040914
NT5E	15	*AREG*	1517.736	*PLAU*	0.040873
DDIT3	14	*ASNS*	1323.028	*CXCL2*	0.040873
RELB	14	*GDF15*	1246.1	*AREG*	0.040821
CD274	14	*KCNQ3*	1190.363	*GDF15*	0.040791
PLAU	13	*ACSL5*	1102	*RELB*	0.040791
CCRL2	13	*STX1A*	1080.531	*BATF3*	0.040781
ASNS	13	*CD274*	947.9778	*CD274*	0.040709
AREG	12	*CD22*	834	*KLF4*	0.040709
IL11	12	*CD24*	811.1906	*IL11*	0.040709
THBD	12	*MMP1*	810.0343	*TRAF1*	0.040709
VEGFC	12	*NRP1*	786.1351	*NT5E*	0.040679
TNFAIP3	12	*SCN5A*	759.8958	*THBD*	0.040679
KLF4	11	*CNIH3*	727.1094	*TNFRSF11B*	0.040659
CD24	11	*VEGFC*	707.3221	*CD24*	0.040638
PLAUR	11	*HSPA5*	665.5574	*MAP2K3*	0.040618
IL33	11	*KLF4*	661.4434	*ZFP36*	0.040588
NR4A1	11	*PLAU*	571.645	*PLAT*	0.040578
IL1RN	11	*RGS2*	556.4	*VEGFC*	0.040557
FOSB	11	*KCNK1*	556	*PLAUR*	0.040557
KITLG	10	*SLC6A9*	533.0405	*KITLG*	0.040547

only qualitatively observed using fluorescence microscopy by staining cells with Hochest 33258. In our study, flow cytometry assay was performed following a more accurate staining method (Annexin V-FITC/PI) to quantitatively determine the percentages of apoptotic and necrotic cells. The high cell death rate was in accordance with decreased cell viability, suggesting reduced metabolic activity of ARPE-19 cells may be attributed to cell loss induced by MWCNTs, which theory can be confirmed in our TEM analysis.[37]

Existing evidence suggests activations of oxidative stress and inflammation are two important factors responsible for MWCNT-induced cytotoxicity.[38–40] ROS levels (an oxidative stress indicator) had been detected to be increased in ARPE-19 cells treated with MWCNTs in the study of Yan et al,[15] while whether inflammation is induced remains unclear. In the present study, we used the transcriptomics analysis to, for the first time, uncover the mechanisms underlying MWNCT-induced retinal toxicity. Similar to previous studies,[38–40] our RNA-seq and bioinformatics analysis found crucial genes (including *CXCL8, MMP1, CASP3, FOS, CXCL2* and *IL11*) associated with MWCNT-induced toxicity in ARPE-19 cells were significantly enriched in inflammation-related GO biological process terms and KEGG pathways. Moreover, CASP3 is a gene that encodes a well-known apoptosis mediator caspase-3. Our PPI network analysis found *CXCL8* could directly interact with *CASP3; CXCL8, IL11* and *CXCL2* could indirectly regulate *CASP3* by interacting with *MMP1; FOS* could interact with *CXCL8, IL11* and *CXCL2*. These findings suggested *FOS*-mediated pro-inflammatory pathways (*FOS-CXCL8*/*IL11*/*CXCL2-MMP1-CASP3*) may be important mechanisms for MWCNT-induced

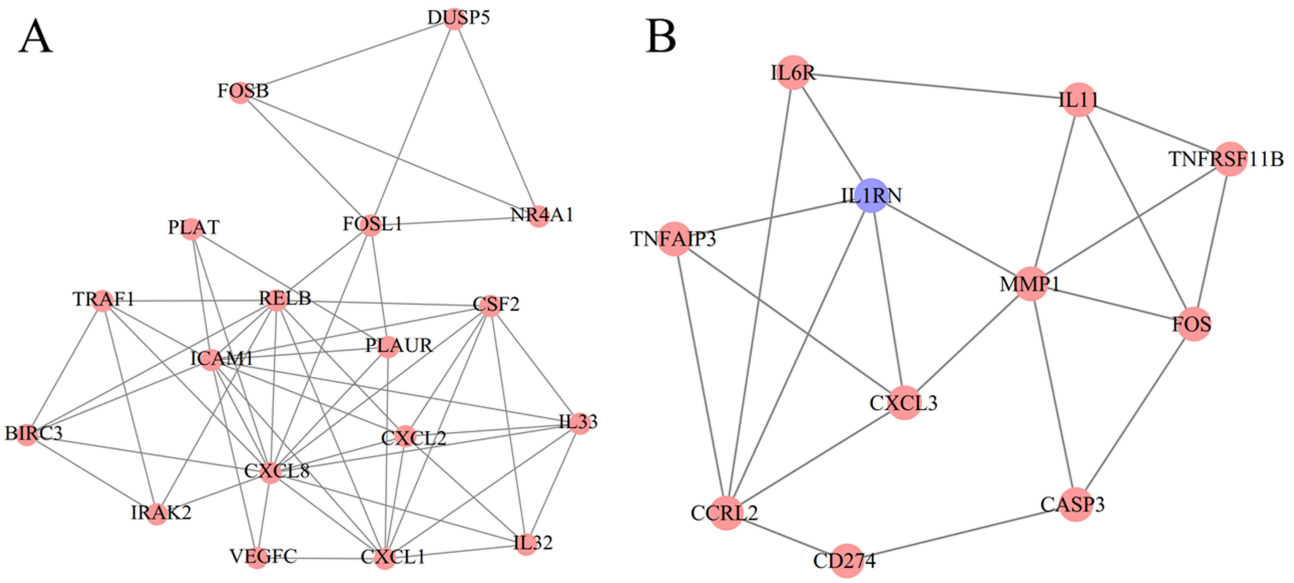

Figure 6 Modules extracted from the protein–protein interaction network. (**A**), module 1; (**B**), module 2. Red indicates upregulated genes; blue indicates downregulated genes.

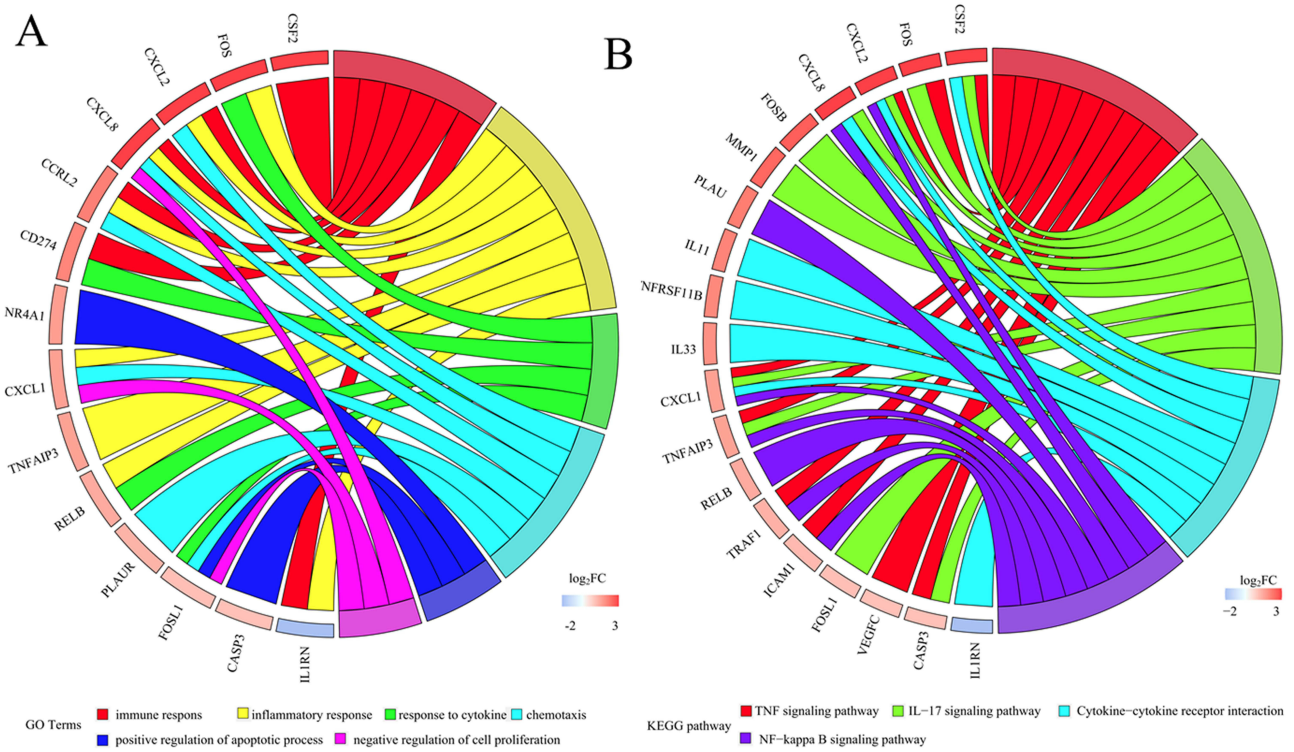

Figure 7 Function enrichment results for hub mRNAs. (**A**), GO biological processes terms; (**B**), KEGG pathways.
Abbreviations: FC, fold change; GO, Gene Ontology; KEGG, Kyoto Encyclopedia of Genes and Genomes.

retinal cell apoptosis and injuries. Some of these genes and their interactions had been reported in MWCNT- or other nanoparticle-exposed cell and animal models, indirectly demonstrating their possible importance for MWCNT-related retinal toxicity. For example, the level of *CXCL8* (also known as IL8) was found to be significantly increased in primary human bronchial epithelial cells,[41] BEAS-2B cell line,[42] human alveolar epithelial A549,[39] primary human hepatocytes with the C3A cell line,[43] human embryonic kidney (HEK293) cells[44] and human renal proximal tubule epithelial cells

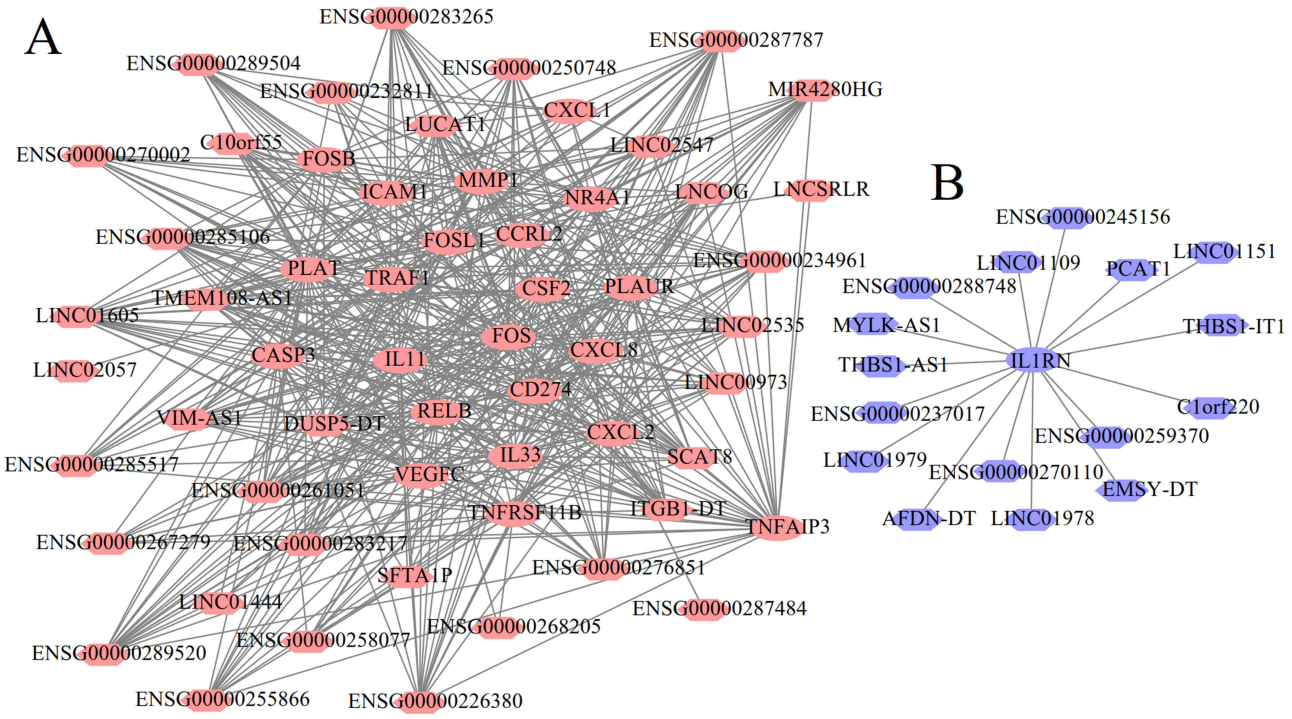

Figure 8 Co-expression networks between lncRNAs and mRNAs. (**A**), relationship pairs for upregulated lncRNAs and mRNAs (red); (**B**), relationship pairs for downregulated lncRNAs and mRNAs (blue). Ellipse indicates the mRNAs; hexagon indicates the lncRNAs.
Abbreviations: LncRNAs, long non-coding RNAs; mRNAs, messenger RNAs.

(HK-2)[45] after they were exposed to MWCNTs. A significant elevation of *CXCL2* was detected in BEAS-2B cells exposed to titanium dioxide nanoparticles[46] and lung tissues of mice exposed to MWCNTs and graphene oxide.[47] *IL11* was identified to be upregulated in human umbilical vein EA.hy926 cell line and BEAS-2B cells exposed to silver nanoparticles.[48] Titanium dioxide nanoparticles were reported to induce an increase in the MMP1 expression at mRNA and protein levels and activity in human pulmonary fibroblasts and this induction was dependent on the activation of its upstream pro-inflammatory pathways, not oxidative stress.[49] The use of an MMP1 inhibitor could abolish the cell apoptosis and necrosis to treat conjunctivochalasis, an inflammatory ocular surface disease.[50] Compared to controls, the transcription of *FOS* was significantly activated in lung, brain and spleen samples by silver[51] and titanium dioxide[52,53] nanoparticles, respectively. Inhibition of c-Fos was proved to suppress the inflammatory reaction, apoptosis[54] and rescue visual function.[55] In line with these studies, we also confirmed all these crucial genes were upregulated at mRNA and protein levels in ARPE-19 cells exposed to MWCNTs.

In the human genome, only 2% of genes are protein-coding, while the remaining transcripts are non-coding RNAs (such as lncRNAs, ≥200 nucleotides in length), which could modulate the expression of protein-coding genes by various mechanisms.[56] Therefore, lncRNAs may also represent crucial biomarkers and targets to interpret the toxicity of nanomaterials.[7,57–59] This hypothesis had been reported by some previous studies: Zhao et al found MWCNTs induced transgenerational toxicity by increasing the expression of germline linc-7, which then activated the downstream transcriptional factor *DAF-12*.[60] Yu et al identified upregulated lncRNA *loc105377478* participated in neodymium oxide nanoparticle-induced injuries in human bronchial epithelial 16HBE cells by enhancing the expression of inflammatory genes *IL6* and *IL8*.[61] Yang et al confirmed nickel oxide nanoparticle exposure downregulated *MEG3* in A549 cells and lung tissues; overexpression of *MEG3* significantly suppressed nanoparticle-induced inflammatory cytokines (IL1β, IL6, TNF-α, CXCL1 and CXCL2).[62] In this study, we screened two crucial lncRNAs *SCAT8* and *LUCAT1* in MWCNT-exposed ARPE-19 cells. Both of them regulated the expression of all FOS-mediated pro-inflammatory pathway genes (*CXCL8, MMP1, CASP3, FOS, CXCL2* and *IL11*). *SCAT8* may be a new gene needed to be further studied because rare studies reported its functions except of one about gastric cancer[63] and one focusing on nasopharyngeal carcinoma.[64]

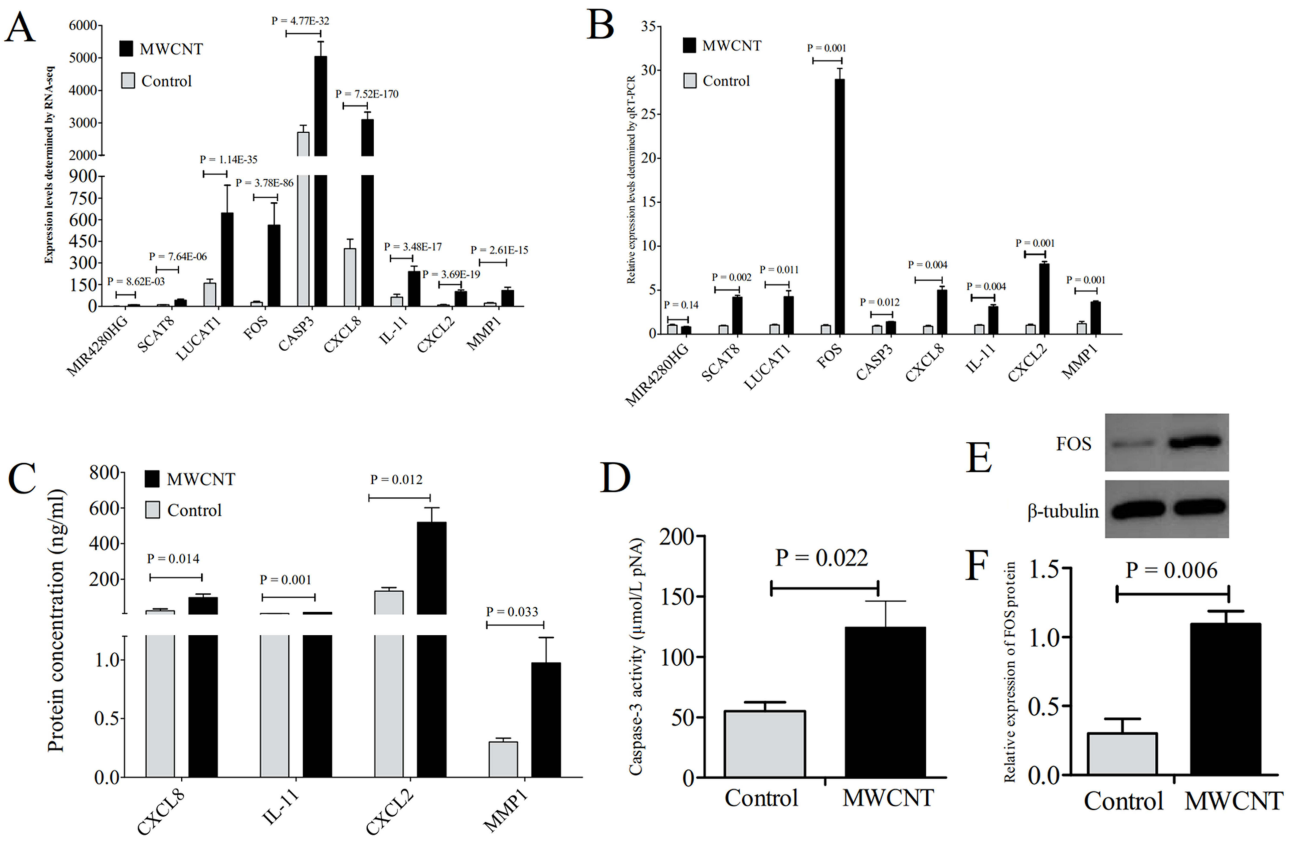

Figure 9 Validation of hub genes induced by MWCNTs in ARPE-19 cells. (**A**), the expression levels of hub genes measured by RNA-seq; (**B**), the relative expression levels of hub genes determined by qRT-PCR; (**C**), the release of CXCL8, MMP1, CXCL2 and IL11 determined by ELISA; (**D**), the caspase-3 enzymatic activity determined by the caspase-3 colorimetric assay kit; (**E**), Western blotting band for FOS protein; (**F**), quantitative expression levels of FOS protein. All results presented are representative of mean ± standard deviations of at least 3 independent experiments. P-value < 0.05 indicates statistical significance.

Abbreviations: CXCL8, C-X-C motif chemokine ligand 8; CXCL2, C-X-C motif chemokine ligand 2; IL11, interleukin 11; MMP1, matrix metallopeptidase 1; CASP3, caspase-3; FOS, Fos proto-oncogene, AP-1 transcription factor subunit; MWCNTs, multi-walled carbon nanotubes.

There had been studies linking lncRNA *LUCAT1* with inflammatory diseases: Zhao et al found *LUCAT1* was upregulated in the serums of chronic obstructive pulmonary disease patients. *LUCAT1* expression was positively correlated with the levels of pro-inflammatory cytokines IL1β, IL6 and TNF-α. *LUCAT1* silencing counteracted the apoptosis- and inflammation-promoting effects of cigarette smoke extract in 16HBE cells.[65] Xiao et al also found knockdown of lncRNA *LUCAT1* suppressed the release of IL1β, IL6 and TNF-α to attenuate sepsis-induced myocardial cell injury.[66] Thus, our theory that *LUCAT1* exerted pro-inflammatory roles to mediate MWCNT-induced toxicity for ARPE-19 cells may be believable.

In addition to ARPE-19 cells, we also validated the toxicity and mechanisms of MWCNTs in another ocular cell type (HCE-T). Similar to ARPE-19, mRNA expression levels of *LUCAT1, MMP1, CXCL2, IL11*, the production of MMP1, CXCL2, IL11 proteins and caspase-3 activity were also validated to be upregulated in HCE-T cells, indicating their changes may be particularly important molecular mechanisms for explaining the ocular toxicity of MWCNTs. Surprisingly, the mRNA and protein expression levels of FOS were found to be downregulated (not upregulated as ARPE-19) in HCE-T cells after being exposed to MWCNTs. This contradictory conclusion may be attributed to the following reasons: 1) different cells may exhibit their own specific response mechanisms; 2) the concentration of 100 μg/mL was not the IC50 for HCE-T, which can be seen in our CCK-8 analysis results (only reduction to 66%). Downregulation of FOS may act as a protective response before IC50 was reached; 3) FOS may have dual functions. The study of Soltysova et al also identified FOS was downregulated in kidney cells after chronic exposure to inorganic nanoparticles.[67]

There were some limitations in this study. First, only ARPE-19 and HCE-T models were used to study the possible toxicological mechanisms of MWCNTs on eyes. Other eye structure-related cells (including retinal ganglion cells,[68] lens

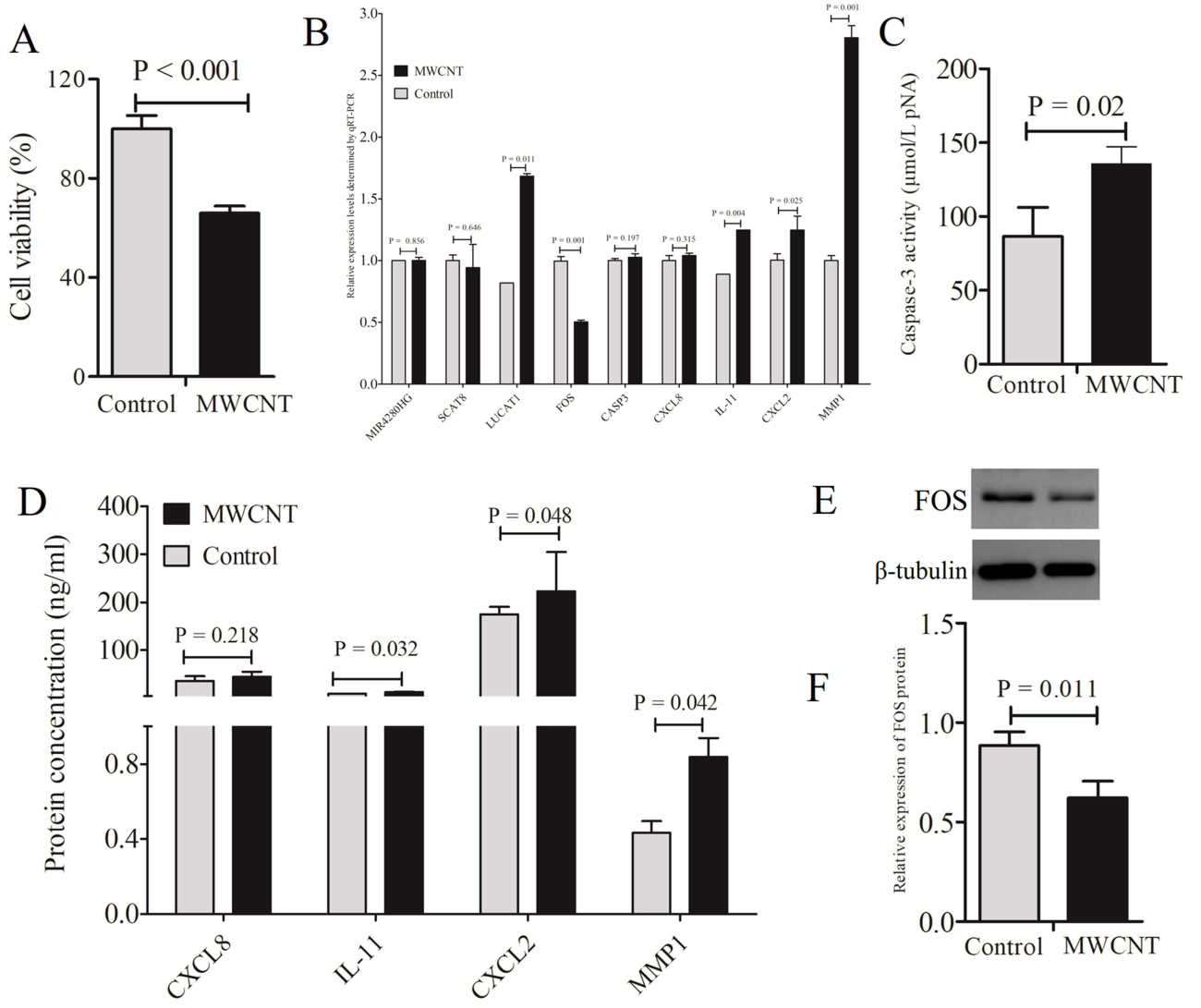

Figure 10 Validation of the toxicity and mechanisms of MWCNTs in HCE-T cells. (**A**), CCK-8 assay detected cell viabilities of HCE-T incubated with MWCNTs for 24 hours; (**B**), qRT-PCR analysis measured the relative expression levels of hub genes identified in ARPE-19 cells; (**C**), ELISA observed the production of CXCL8, MMP1, CXCL2 and IL11; (**D**), colorimetric analysis determined the caspase-3 enzymatic activity; (**E**), Western blotting band for FOS protein; (**F**), quantitative expression levels of FOS protein. All results presented are representative of mean ± standard deviations of three independent experiments. *P*-value < 0.05 indicates statistical significance.
Abbreviations: CXCL8, C-X-C motif chemokine ligand 8; CXCL2, C-X-C motif chemokine ligand 2; IL11, interleukin 11; MMP1, matrix metallopeptidase 1; CASP3, caspase-3; FOS, Fos proto-oncogene, AP-1 transcription factor subunit; MWCNTs, multi-walled carbon nanotubes.

epithelial cells,[69] photoreceptor cells)[70] and animal models (acute intravitreal injection,[68] conjunctival sac injection[71] and chronic whole-body airborne exposure modelling the occupational environment)[72] should be established to further confirm the importance of our identified genes for MWCNT-induced eye injuries. Second, the regulatory relationships among genes in FOS-mediated pro-inflammatory pathway and the upstream roles of lncRNAs *LUCAT1* and *SCAT8* need to be verified by wet experiments (eg, co-precipitation, silencing or overexpression). Third, in addition to directly regulating the target genes, lncRNAs are also known to function as competing endogenous RNAs (ceRNAs) to sponge microRNAs and then regulate the target genes of microRNAs.[7,73] Only one significant miRNA was identified in our transcriptomics study (miR-647: $\log_2$FC = −1.7, FDR = 5.27E-04), but which was found not to be significant by qRT-PCR (data not shown). Thus, miRNA deep-sequencing is required to screen hub miRNAs associated with MWCNT-induced eye injuries and reveal the function mechanisms of *LUCAT1* and *SCAT8* as ceRNAs. Fourth, in consideration of differential expression in our identified genes between ARPE-19 and HCE-T cell models, RNA-sequencing was necessary for HCE-T and other ocular cells to screen the shared genes, which may be particularly vital to serve as

monitoring biomarkers and therapeutic targets for human beings exposed to MWCNTs. Fifth, the toxicity and mechanisms of pristine and functionalized MWCNTs should be compared in various ocular cells.[74] Sixth, in addition to apoptosis and necroptosis, recent studies showed activation of pyroptosis may be also important mechanisms associated with cell damages induced by nanomaterials.[75,76] However, our RNA-sequencing results revealed the pyroptosis-related genes, including caspase 1 (*CASP*1; $\log_2$FC = −0.28, p-value = 0.27, FDR = 0.44), NLR family pyrin domain containing 3 (*NLRP3*; not included in dataset), gasdermin D (*GSDMD*; $\log_2$FC = −0.33; p-value = 1.15E-03, FDR = 6.51E-03) and interleukin 1 beta (*IL1B*; $\log_2$FC = −0.52; p-value = 0.31, FDR = 0.49) were not significantly differentially expressed after MWCNT exposure in ARPE-19 cells. Thus, whether pyroptosis is involved in the toxic mechanism of MWCNTs in ocular cells needs experimental confirmation in the future.

Conclusion

In summary, we employed the ARPE-19 and HCE-T cell model to determine the ocular toxicity of pristine MWCNTs and the underlying mechanisms. Our results found that exposure to small-diameter MWCNTs (7–11 nm) induced cytotoxicity on ARPE-19 cells, with significantly decreased cell viability and increased percentages of apoptotic and necrotic cells. Transcriptomics analysis and wet experiments indicated upregulation of FOS-mediated pro-inflammatory pathway genes (*CXCL8, MMP1, CXCL2* and *IL11*) may be responsible for MWCNT-induced ARPE-19 cell death (as evidenced by their interactions with the apoptosis biomarker *CASP3*), while lncRNAs *LUCAT1* and *SCAT8* were their upstream regulatory factors. The reduced cell viability and increased caspase-3 activity and the expression of *LUCAT1, MMP1, CXCL2*, and *IL11* at mRNA and protein levels were also validated in HCE-T cells exposed to MWCNTs. These shared genes in two ocular cells may represent potential biomarkers for monitoring MWCNT-induced eye disorders and targets for developing preventive and therapeutic strategies in the future.

Data Sharing Statement

Data analyzed are available from the corresponding authors on request.

Funding

Financial support from National Key Research and Development Program of China (2017YFA0204600) and Project funded by China Postdoctoral Science Foundation (2017M621322, 2018T110324) is greatly acknowledged.

Disclosure

The authors declare no competing interests.

References

1. Li J, Xin M, Ma Z, Shi Y, Pan L. Nanomaterials and their applications on bio-inspired wearable electronics. *Nanotechnology*. 2021;32(47):472002.
2. Luo X, Liang Y, Weng W, Hu Z, Zhu M. Polypyrrole-coated carbon nanotube/cotton hybrid fabric with high areal capacitance for flexible quasi-solid-state supercapacitors. *Energy Storage Mater*. 2020;33(2020):11–17.
3. Ranjha M, Shafique B, Rehman A, et al. Biocompatible nanomaterials in food science, technology, and nutrient drug delivery: recent developments and applications. *Front Nutr*. 2022;8:778155.
4. Bhat BB, Kamath PP, Chatterjee S, Bhattacherjee R, Nayak UY. Recent updates on nanocosmeceutical skin care and anti-aging products. *Curr Pharm Des*. 2022;28(15):1258–1271.
5. Zhu S, Gong L, Li Y, Xu H, Gu Z, Zhao Y. Safety assessment of nanomaterials to eyes: an important but neglected issue. *Adv Sci*. 2019;6(16):1802289.
6. Bae JS, Oh SB, Kim J, et al. Particulate matter exposure aggravates IL-17-induced eye and nose inflammation in an OVA/Poly (I:C) mouse model. *Allergy Asthma Immunol Res*. 2022;14(1):59–72.
7. Xie D, Hu J, Wu T, Cao K, Luo X. Potential Biomarkers and drugs for nanoparticle-induced cytotoxicity in the retina: based on regulation of inflammatory and apoptotic genes. *Int J Environ Res Public Health*. 2022;19(9):5664.
8. Yang R, Yang S, Li K, et al. Carbon nanotube polymer scaffolds as a conductive alternative for the construction of retinal sheet tissue. *ACS Chem Neurosci*. 2021;12(17):3167–3175.
9. Eleftheriou CG, Zimmermann JB, Kjeldsen HD, David-Pur M, Hanein Y, Sernagor E. Carbon nanotube electrodes for retinal implants: a study of structural and functional integration over time. *Biomaterials*. 2017;112:108–121.
10. Sharma S, Bhatia V. Nanoscale drug delivery systems for glaucoma: experimental and in silico advances. *Curr Top Med Chem*. 2021;21(2):115–125.
11. El-Gendy AO, Obaid Y, Ahmed E, Enwemeka CS, Hassan M, Mohamed T. The antimicrobial effect of gold quantum dots and femtosecond laser irradiation on the growth kinetics of common infectious eye pathogens: an in vitro study. *Nanomaterials*. 2022;12(21):3757.

12. El-Gendy AO, Nawaf KT, Ahmed E, et al. Preparation of zinc oxide nanoparticles using laser-ablation technique: retinal epithelial cell (ARPE-19) biocompatibility and antimicrobial activity when activated with femtosecond laser. *J Photochem Photobiol B*. 2022;234:112540.
13. Wang J, Xu Y, Yang Z, et al. Toxicity of carbon nanotubes. *Curr Drug Metab*. 2013;14(8):891–899.
14. Yan L, Zhang S, Zeng C, et al. Cytotoxicity of single-walled carbon nanotubes with human ocular cells. *Adv Mater Res*. 2011;287–290:32–36.
15. Yan L, Li GX, Zhang S, et al. Cytotoxicity and genotoxicity of multi-walled carbon nanotubes with human ocular cells. *Chin Sci Bulletin*. 2013;58:2347–2353.
16. Kishore AS, Surekha P, Murthy PB. Assessment of the dermal and ocular irritation potential of multi-walled carbon nanotubes by using in vitro and in vivo methods. *Toxicol Lett*. 2009;191(2–3):268–274.
17. Kataoka C, Nakahara K, Shimizu K, et al. Salinity-dependent toxicity of water-dispersible, single-walled carbon nanotubes to Japanese medaka embryos. *J Appl Toxicol*. 2017;37(4):408–416.
18. Strauss O. The retinal pigment epithelium in visual function. *Physiol Rev*. 2005;85(3):845–881.
19. Dobin A, Davis CA, Schlesinger F, et al. STAR: ultrafast universal RNA-seq aligner. *Bioinformatics*. 2013;29(1):15–21.
20. Anders S, Pyl PT, Huber W. HTSeq–a Python framework to work with high-throughput sequencing data. *Bioinformatics*. 2015;31(2):166–169.
21. Anders S, Huber W. Differential expression analysis for sequence count data. *Genome Biol*. 2010;11(10):R106.
22. Langfelder P, Horvath S. WGCNA: an R package for weighted correlation network analysis. *BMC Bioinform*. 2008;9:559.
23. Szklarczyk D, Franceschini A, Wyder S, et al. STRING v10: protein-protein interaction networks, integrated over the tree of life. *Nucleic Acids Res*. 2015;43(Databaseissue):D447–452.
24. Tang Y, Li M, Wang J, Pan Y, Wu FX. CytoNCA: a cytoscape plugin for centrality analysis and evaluation of protein interaction networks. *Biosystems*. 2015;127:67–72.
25. Bader GD, Hogue CW. An automated method for finding molecular complexes in large protein interaction networks. *BMC Bioinform*. 2003;4:2.
26. Jin X, Xue B, Zhou Q, Su R, Li Z. Mitochondrial damage mediated by ROS incurs bronchial epithelial cell apoptosis upon ambient PM2.5 exposure. *J Toxicol Sci*. 2018;43(2):101–111.
27. Chen X, Zhu S, Hu X, et al. Toxicity and mechanism of mesoporous silica nanoparticles in eyes. *Nanoscale*. 2020;12(25):13637–13653.
28. Numano T, Sugiyama T, Kawabe M, et al. Lung toxicity of a vapor-grown carbon fiber in comparison with a multi-walled carbon nanotube in F344 rats. *J Toxicol Pathol*. 2021;34(1):57–71.
29. Lucas JH, Wang Q, Muthumalage T, Rahman I. Multi-Walled Carbon Nanotubes (MWCNTs) cause cellular senescence in TGF-β stimulated lung epithelial cells. *Toxics*. 2021;9(6):144.
30. Awogbindin IO, Maduako IC, Adedara IA, et al. Kolaviron ameliorates hepatic and renal dysfunction associated with multiwalled carbon nanotubes in rats. *Environ Toxicol*. 2021;36(1):67–76.
31. Samiei F, Shirazi FH, Naserzadeh P, Dousti F, Seydi E, Pourahmad J. Toxicity of multi-wall carbon nanotubes inhalation on the brain of rats. *Environ Sci Pollut Res Int*. 2020;27(11):12096–12111.
32. Adedara IA, Awogbindin IO, Maduako IC, et al. Kolaviron suppresses dysfunctional reproductive axis associated with multi-walled carbon nanotubes exposure in male rats. *Environ Sci Pollut Res Int*. 2021;28(1):354–364.
33. Zhao X, Chang S, Long J, Li J, Li X, Cao Y. The toxicity of multi-walled carbon nanotubes (MWCNTs) to human endothelial cells: the influence of diameters of MWCNTs. *Food Chem Toxicol*. 2019;126:169–177.
34. Fujita K, Obara S, Maru J, Endoh S. Cytotoxicity profiles of multi-walled carbon nanotubes with different physico-chemical properties. *Toxicol Mech Methods*. 2020;30(7):477–489.
35. Wang X, Jia G, Wang H, et al. Diameter effects on cytotoxicity of multi-walled carbon nanotubes. *J Nanosci Nanotechnol*. 2009;9(5):3025–3033.
36. Poulsen SS, Jackson P, Kling K, et al. Multi-walled carbon nanotube physicochemical properties predict pulmonary inflammation and genotoxicity. *Nanotoxicology*. 2016;10(9):1263–1275.
37. Gali NK, Ning Z, Daoud W, Brimblecombe P. Investigation on the mechanism of non-photocatalytically TiO_2-induced reactive oxygen species and its significance on cell cycle and morphology. *J Appl Toxicol*. 2016;36(10):1355–1363.
38. Wils RS, Jacobsen NR, Vogel U, Roursgaard M, Møller P. Inflammatory response, reactive oxygen species production and DNA damage in mice after intrapleural exposure to carbon nanotubes. *Toxicol Sci*. 2021;183(1):184–194.
39. Di Ianni E, Erdem JS, Møller P, et al. In vitro-in vivo correlations of pulmonary inflammogenicity and genotoxicity of MWCNT. *Part Fibre Toxicol*. 2021;18(1):25.
40. de Godoy KF, de Almeida Rodolpho JM, Brassolatti P, et al. New multi-walled carbon nanotube of industrial interest induce cell death in murine fibroblast cells. *Toxicol Mech Methods*. 2021;31(7):517–530.
41. Hussain S, Sangtian S, Anderson SM, et al. Inflammasome activation in airway epithelial cells after multi-walled carbon nanotube exposure mediates a profibrotic response in lung fibroblasts. *Part Fibre Toxicol*. 2014;11:28.
42. Ursini CL, Maiello R, Ciervo A, et al. Evaluation of uptake, cytotoxicity and inflammatory effects in respiratory cells exposed to pristine and -OH and -COOH functionalized multi-wall carbon nanotubes. *J Appl Toxicol*. 2016;36(3):394–403.
43. Kermanizadeh A, Gaiser BK, Ward MB, Stone V. Primary human hepatocytes versus hepatic cell line: assessing their suitability for in vitro nanotoxicology. *Nanotoxicology*. 2013;7(7):1255–1271.
44. Reddy AR, Reddy YN, Krishna DR, Himabindu V. Multi wall carbon nanotubes induce oxidative stress and cytotoxicity in human embryonic kidney (HEK293) cells. *Toxicology*. 2010;272(1–3):11–16.
45. Kermanizadeh A, Vranic S, Boland S, et al. An in vitro assessment of panel of engineered nanomaterials using a human renal cell line: cytotoxicity, pro-inflammatory response, oxidative stress and genotoxicity. *BMC Nephrol*. 2013;14:96.
46. Park EJ, Yi J, Chung KH, Ryu DY, Choi J, Park K. Oxidative stress and apoptosis induced by titanium dioxide nanoparticles in cultured BEAS-2B cells. *Toxicol Lett*. 2008;180(3):222–229.
47. Danielsen PH, Bendtsen KM, Knudsen KB, Poulsen SS, Stoeger T, Vogel U. Nanomaterial- and shape-dependency of TLR2 and TLR4 mediated signaling following pulmonary exposure to carbonaceous nanomaterials in mice. *Part Fibre Toxicol*. 2021;18(1):40.
48. Jang J, Park S, Choi IH. Increased interleukin-11 and stress-related gene expression in human endothelial and bronchial epithelial cells exposed to silver nanoparticles. *Biomolecules*. 2021;11(2):234.
49. Armand L, Dagouassat M, Belade E, et al. Titanium dioxide nanoparticles induce matrix metalloprotease 1 in human pulmonary fibroblasts partly via an interleukin-1β-dependent mechanism. *Am J Respir Cell Mol Biol*. 2013;48(3):354–363.

50. Guo P, Zhang SZ, He H, Zhu YT, Tseng SC. PTX3 controls activation of matrix metalloproteinase 1 and apoptosis in conjunctivochalasis fibroblasts. *Invest Ophthalmol Vis Sci*. 2012;53(7):3414–3423.
51. Asare N, Duale N, Slagsvold HH, et al. Genotoxicity and gene expression modulation of silver and titanium dioxide nanoparticles in mice. *Nanotoxicology*. 2016;10(3):312–321.
52. Sheng L, Wang L, Su M, et al. Mechanism of TiO2 nanoparticle-induced neurotoxicity in zebrafish (Danio rerio). *Environ Toxicol*. 2016;31(2):163–175.
53. Sang X, Li B, Ze Y, et al. Toxicological mechanisms of nanosized titanium dioxide-induced spleen injury in mice after repeated peroral application. *J Agric Food Chem*. 2013;61(23):5590–5599.
54. Zhou L, Xue C, Chen Z, Jiang W, He S, Zhang X. c-Fos is a mechanosensor that regulates inflammatory responses and lung barrier dysfunction during ventilator-induced acute lung injury. *BMC Pulm Med*. 2022;22(1):9.
55. Sun Y, Lin Z, Liu CH, et al. Inflammatory signals from photoreceptor modulate pathological retinal angiogenesis via c-Fos. *J Exp Med*. 2017;214 (6):1753–1767.
56. Gil N, Ulitsky I. Regulation of gene expression by cis-acting long non-coding RNAs. *Nat Rev Genet*. 2020;21(2):102–117.
57. Ndika J, Karisola P, Kinaret P, Ilves M, Alenius H. Profiling non-coding RNA changes associated with 16 different engineered nanomaterials in a mouse airway exposure model. *Cells*. 2021;10(5):1085.
58. Chang G, Xie D, Hu J, Wu T, Cao K, Luo X. Identification of candidate lncRNA and pseudogene biomarkers associated with carbon-nanotube-induced malignant transformation of lung cells and prediction of potential preventive drugs. *Int J Environ Res Public Health*. 2022;19(5):2936.
59. Xue D, Zou W, Liu D, et al. Cytotoxicity and transcriptome changes triggered by CuInS(2)/ZnS quantum dots in human glial cells. *Neurotoxicology*. 2022;88:134–143.
60. Zhao Y, Xu R, Hua X, Rui Q, Wang D. Multi-walled carbon nanotubes induce transgenerational toxicity associated with activation of germline long non-coding RNA linc-7 in. *C Elegans Chemosph*. 2022;301:134687.
61. Yu F, Zhang X, Gao L, et al. LncRNA loc105377478 promotes NPs-Nd_2O_3-induced inflammation in human bronchial epithelial cells through the ADIPOR1/NF-κB axis. *Ecotoxicol Environ Saf*. 2021;208:111609.
62. Yang M, Chang X, Gao Q, et al. LncRNA MEG3 ameliorates NiO nanoparticles-induced pulmonary inflammatory damage via suppressing the p38 mitogen activated protein kinases pathway. *Environ Toxicol*. 2022;37(5):1058–1070.
63. Wu H, Zhou J, Chen S, Zhu L, Jiang M, Liu A. Survival-related lncRNA landscape analysis identifies LINC01614 as an oncogenic lncRNA in gastric cancer. *Front Genet*. 2021;12:698947.
64. Jiang C, Feng D, Zhang Y, Yang K, Hu X, Xie Q. SCAT8/miR-125b-5p axis triggers malignant progression of nasopharyngeal carcinoma through SCARB1. *BMC Mol Cell Biol*. 2023;24(1):15.
65. Zhao S, Lin C, Yang T, Qian X, Lu J, Cheng J. Expression of long non-coding RNA LUCAT1 in patients with chronic obstructive pulmonary disease and its potential functions in regulating cigarette smoke extract-induced 16HBE cell proliferation and apoptosis. *J Clin Lab Anal*. 2021;35(7):e23823.
66. Wang J, Xin S, Yang R, Jiang J, Qiao Y. Knockdown of lncRNA LUCAT1 attenuates sepsis-induced myocardial cell injury by sponging miR-642a. *Mamm Genome*. 2021;32(6):457–465.
67. Soltysova A, Begerova P, Jakic K, et al. Genome-wide DNA methylome and transcriptome changes induced by inorganic nanoparticles in human kidney cells after chronic exposure. *Cell Biol Toxicol*. 2022;2022:1–8.
68. Zhang Z, Zhao L, Ma Y, et al. Mechanistic study of silica nanoparticles on the size-dependent retinal toxicity in vitro and in vivo. *J Nanobiotechnology*. 2022;20(1):146.
69. Hanafy BI, Cave GWV, Barnett Y, Pierscionek B. Treatment of human lens epithelium with high levels of nanoceria leads to reactive oxygen species mediated apoptosis. *Molecules*. 2020;25(3):441.
70. Wang L, Chen C, Guo L, et al. Zinc oxide nanoparticles induce murine photoreceptor cell death via mitochondria-related signaling pathway. *Artif Cells Nanomed Biotechnol*. 2018;46(sup1):1102–1113.
71. An W, Zhang Y, Zhang X, et al. Ocular toxicity of reduced graphene oxide or graphene oxide exposure in mouse eyes. *Exp Eye Res*. 2018;174:59–69.
72. Sager TM, Umbright CM, Mustafa GM, et al. Pulmonary toxicity and gene expression changes in response to whole-body inhalation exposure to multi-walled carbon nanotubes in rats. *Inhal Toxicol*. 2022;34(7–8):200–218.
73. Fu Y, Li B, Yun J, et al. lncRNA SOX2-OT ceRNA network enhances the malignancy of long-term $PM_{2.5}$-exposed human bronchial epithelia. *Ecotoxicol Environ Saf*. 2021;217:112242.
74. Abu Gazia M, El-Magd MA. Effect of pristine and functionalized multiwalled carbon nanotubes on rat renal cortex. *Acta Histochem*. 2019;121 (2):207–217.
75. Sallam AA, El-Magd MA, Ahmed MM, et al. Quercetin alleviated multi-walled carbon nanotubes-induced neurotoxicity in mice through inhibition of oxidation, inflammation, and pyroptosis. *Biomed Pharmacother*. 2022;151:113160.
76. Pei X, Jiang H, Li C, Li D, Tang S. Oxidative stress-related canonical pyroptosis pathway, as a target of liver toxicity triggered by zinc oxide nanoparticles. *J Hazard Mater*. 2023;442:130039.